Published in final edited form as:
Cancer Metastasis Rev. 2008 December ; 27(4): 589–613. doi:10.1007/s10555-008-9157-4.

Imaging Hemodynamics

Dominique Jennings[1], **Natarajan Raghunand**[4], and **Robert J. Gillies**[1,2,3,4]

Dominique Jennings: djenning@email.arizona.edu; Natarajan Raghunand: raghunan@email.arizona.edu; Robert J. Gillies: gillies@email.arizona.edu

[1]Department of Biomedical Engineering, The University of Arizona, Tucson, Arizona

[2]Department of Physiology, The University of Arizona, Tucson, Arizona

[3]Department of Biochemistry, The University of Arizona, Tucson, Arizona

[4]Department of Radiology, The University of Arizona, Tucson, Arizona

Abstract

Microvascular permeability is a pharmacologic indicator of tumor response to therapy, and it is expected that this biomarker will evolve into a clinical surrogate endpoint and be integrated into protocols for determining patient response to antiangiogenic or antivascular therapies. This review discusses the physiological context of vessel permeability in an imaging setting, how it is affected by active and passive transport mechanisms, and how it is described mathematically for both theoretical and complex dynamic microvessel membranes. Many research groups have established dynamic-enhanced imaging protocols for estimating this important parameter. This review discusses those imaging modalities, the advantages and disadvantages of each, and how they compare in terms of their ability to deliver information about therapy-associated changes in microvessel permeability in humans. Finally, this review discusses future directions and improvements needed in these areas.

1 Introduction to Hemodynamics

1.1 Defining Vascular Permeability and Perfusion

Perfusion is the process by which the circulatory system delivers blood to tissues. It is mathematically equivalent to flow, expressed in mL $100g^{-1}$ tissue min^{-1}. By Poiseuille's Law, flow is a function of the pressure gradient over a given length of vessel and the resistance of that vessel to the flow of viscous fluid (blood). By contrast, vascular permeability is expressed as a transfer coefficient of a solute per unit time, per volume of tissue between the vascular compartment (plasma) and the extracellular extravascular space (EES). Permeability has the units cm sec^{-1} and is functionally equivalent to a diffusion coefficient (cm^2 sec^{-1}) corrected for the presence of an intervening semi-permeable membrane.

1.2 Macrocirculation – Overview

1.2.1. Morphology—A physiologically normal blood vessel is an unctuous conduit for blood flow. Both arteries and veins have three identifiable or distinct layers: *tunica intima, media and adventitia* [1]. The *tunica intima* is the innermost layer or the layer most proximal to the lumen of the vessel and itself is composed of three layers: the endothelium,

subendothelial layer and the internal elastic membrane. The endothelium is a confluent monolayer of endothelial cells that are aligned in the direction of flow. The abluminal surface of the endothelial layer is embedded by a basement membrane (subendothelial layer) composed of collagen, fibronectin and laminin. In some vessels, the basement membrane may rest directly on the internal elastic membrane. This membrane interfaces with the central layer or the *tunica media.*

The *tunica media* constitutes the greatest volume for the vessel, comprised mainly of smooth muscle cells. In arteries, one may also find reticular collagenous fibers and an external elastic membrane, all of which regulate the vasoconstrictive and vasodilatory properties of the vessel important for maintaining blood pressure. In veins, besides smooth muscle cells, one may only find fibroelastic connective tissue.

The outermost layer of the vessel, the *tunica adventitia* is comprised mostly of collagenous tissue, nerves and fibroblasts [1]. Arterial adventitia sometimes presents with a vascular network known as the vasa vasorum. In the veins, however, there is evidence of connective tissue, fibroblasts, elastic fibers and smooth muscle cells. Another distinct difference between veins and arteries is that veins may possess valves which prevent reflux of blood. The anatomical differences between veins and arteries are diagrammed in Figure 1.

1.2.2. Vessel Regulation of Flow—A pressure gradient (expressed in mm Hg) down the vessel imparts flow [2]. Flow (F, ml sec^{-1}), is the product of the blood flow velocity, ν, or displacement of blood per unit time (cm sec^{-1}) and the cross-sectional area of the vessel (A, cm^2): $F = \nu \cdot A$. The characteristic hierarchal branching of the cardiovascular system is designed such that the more extensive the branching, the greater the cross-sectional area. As the total flow rate must remain constant throughout the system, the blood flow velocity, ν, must decrease as it moves through arteries and arterioles down to the capillary level [2].

Resistance is another important factor that affects blood flow. Hemodynamic resistance is a measure of the opposition to blood flow through a vessel [2]. Throughout the cardiovascular system, pressure increases with increased resistance to maintain a constant flow rate. Resistance is dependent on: 1) blood viscosity, η; 2) vessel length, and; 3) vessel radius [1]. Although the viscosity of blood is shear-rate dependent, it remains relatively constant throughout the vascular system and therefore, does not contribute a great deal to the control of resistance. Similarly, the length of vessels in a system is also constant. Thus, the main variable determinant of resistance is vessel radius. A small change in the radius leads to a significant change in flow as resistance is inversely proportional to the fourth power of the radius:

$$R \propto \frac{1}{r^4} \quad \text{Equation 1}$$

The greatest control over vessel radii, and hence resistance, occurs at the level of the arteriole. This is because extensive downstream capillary branching leads to a steep post-arteriole pressure gradient.

Poiseuilles's Law describes the flow rate Φ (mL sec^{-1}) of an incompressible fluid as:

$$\Phi = \frac{\pi \Delta P r^4}{8 \eta L}, \quad \text{Equation 2}$$

where $\Delta P/L$ represents the pressure gradient ($P_1 - P_2$) over a given length, L. Poiseuilles's Law is limited by a few assumptions: 1) the radius of the tube must be constant, and much smaller than the length of the tube, 2) the fluid viscosity must be uniform and constant, 3) flow is laminar, and, 4) the velocity at the tube edge is zero or negligible. The second and third assumptions may not be met in the arterial circulation and hence, Poiseuilles's Law is only a useful approximation of total blood flow [2].

1.3 Capillary Microcirculation

Imaging studies of vascular permeability primarily reflect microcirculatory (capillary) phenomena. It is estimated that the human body is equipped with 10–40 billion capillaries, which provide over 600 m^2 of surface area for exchange of materials. Capillary walls are thin (~1 μm) and the average diameter of a capillary is small (~3 μm) compared to that of a red blood cell (~8 μm). In normal tissues, the abundance of capillaries is such that no cell is farther than 100 μm away from a capillary [2]. Extensive data have shown that this is clearly not the case in tumors (described below).

There are fewer cell types comprising capillaries compared to other vessels, but the underlying biology of the cells is more complex. A single, flat layer of endothelial cells joined together by tight junctions constitutes the inner lining of capillaries, and these cells are as heterogeneous as the tissues they perfuse. Oh et al. developed a discovery and validation approach to understand the heterogeneity in lung endothelial cells [3,4]. This productive research led to discovery of about 50 differentially expressed proteins, two of which may permit immuno-targeting and imaging *in vivo*. An outer basement membrane surrounds these cells, and in some capillary beds, perivascular cells or pericytes surround that basement membrane.

Capillary endothelia are categorized according to porosity. *Continuous* capillaries are the most common, and maintain a tight barrier between the blood and the interstitial fluid. These are observed in tissues that require a significant amount of protection from blood constituents such as the central nervous system, muscle and lung. *Fenestrated* capillaries are more porous, with clefts between endothelial cells and fenestrations at the surface of the endothelial cells. These allow passage of water-soluble substances such as glucose and amino acids, but they are not permeable to plasma proteins. Fenestrae can be completely open, like a pore, or may be covered by a thin, non-membranous diaphragm across the opening. *Sinusoidal* capillaries are specialized vessels found in organs (e.g. bone marrow, spleen or liver) that require the involution or excretion of whole cells, large molecules or assorted particles from the blood. The diameters of these capillaries are large (~50 μm). The lumen is irregularly shaped and lined by specialized phagocytic cells. These vessels have large intercellular clefts and fenestrations that lack diaphragms. In some vessels the basal lamina may be partially or completely absent. Of all microcirculatory vessel types, these sinusoidal vessels most resemble capillaries found in tumors.

1.3.1. Passive Capillary Transport—Poiseuille's Law is useful for describing the flow of whole blood through blood vessels. Both plasma and solute molecules contained in blood also undergo passive transport across the capillary wall, by either diffusive or convective mechanisms [1]. Active transport mechanisms are discussed later in this review. In solution or in tissues without a permeability barrier, Fick's law of diffusion simply states:

$$\frac{dQ}{dt} = -DS\frac{\partial C}{\partial x}, \quad \text{Equation 3}$$

where dQ is the diffusive flux (mmol) in time dt across a plane of area, S (cm^2), under an instantaneous concentration gradient (∂C, mmol cm^{-3}, ∂x, cm^{-1}), and D is the diffusion coefficient (cm^2 sec^{-1}) at a given temperature in a given medium [5].

The expression changes in the context of two compartments (C_1 and C_2) separated by a semi-permeable membrane. Across the membrane, Q depends on permeability of the membrane to the materials being exchanged, and the ratio of the area (S) to the thickness (H) of the membrane becomes important:

$$\frac{dQ}{dt} = -D\frac{S}{H}(C_1 - C_2). \quad \text{Equation 4}$$

This model assumes that compartments C_1 and C_2 are homogenous and perfectly mixed, and diffusion occurs only in the membrane. In the treatment of a capillary and its surrounding stroma, or the interstitial space, these conditions are met, and modeling permeability of the capillary membrane requires that the influence of diffusion on the tracer becomes negligible and that the two compartments (vascular and interstitial compartments) are well mixed at all times. Through simple mass balance, uptake of tracer in tissue can be expressed as the difference between the quantity of tracer delivered to the tissue from the arterial phase (C_a) and the quantity removed by the venous phase (C_v):

$$Q = F(C_a - C_v). \quad \text{Equation 5}$$

These concepts are developed more extensively in the treatment of Dynamic Contrast-Enhanced MRI estimation of tracer concentration later in this review.

1.4 Angiogenesis

Angiogenesis is an important component of tumor formation. The angioblast is commonly believed to be the progenitor of endothelial cells, yet a multipotential precursor, the hemangioblast, has been identified that can differentiate into either hematopoietic or endothelial cells [6]. Recent studies have confirmed an alternative pathway not involving erythropoiesis [7,8,9], though it remains unclear when the divergence of these two lineages occurs.

Vasculogenesis is the differentiation of the angioblast in the embryonic and extra-embryonic mesoderm and subsequent formation of primordial capillary plexus from angioblasts at their site of origin [10]. Vascular endothelial growth factor (VEGF) and its associated receptors,

VEGF-Receptor 1 and 2 (VEGF-R1 and -R2) and the angiopoietin/Tie receptor system are the known principal endothelium-specific factors and associated receptors that regulate vasculogenesis during embryogenesis [11]. Following successful elaboration of the cardiovascular system, the expansion of the microvasculature in embryogenesis (and in adult tissue remodeling) occurs by angiogenesis. During normal, post-natal development, there is little need for angiogenesis except during reproductive cycling and wound healing [12,13,14,15]. Angiogenesis on an established vascular scaffold includes pruning of pre-existing vessels and the formation of new capillaries, by both sprouting and non-sprouting angiogenesis (intussusception) [16,17,18,19].

Sprouting angiogenesis is a relatively slow process characterized by the extension of capillary sprouts invading the mesenchyme. Sprouting is initiated by the proteolytic degradation of the basement membrane on an established capillary, followed by the migration and proliferation of endothelial cells into the extracellular matrix and along the chemotactic gradient to a proximal capillary. The sprouts internally reorganize to create a vascular lumen and form a stable connection with an adjacent capillary. Though the entire extension process requires little more than 24 hours, perfusion of the new capillary does not occur for 3–5 days following its inauguration into the vascular system [19].

1.4.1. Molecular Mechanisms of Angiogenesis—Mediators of angiogenesis have excitatory or inhibitory effects on vessel initiation and growth. These mediators vary spatially and temporally throughout the angiogenic process, and this differential regulation generally manifests as an inhibition of angiogenesis at any given point in time [20,21]. If new vessel growth or remodeling is required, this inhibition is attenuated and activators of angiogenesis are expressed and mobilized. The entire process of angiogenesis can be organized into two general categories: initiation and resolution [22,23]. The *initiation* process constitutes a period of growth and expansion following a stimulus to generate, expand or remodel the local vasculature. The *resolution* phase involves the stabilization of nascent blood vessels by reinstatement of balanced levels of angiogenic growth factors that favor angiogenic quiescence. Both processes are tightly regulated and inextricably linked to one another.

The initiation phase of angiogenesis is characterized by endothelial cell activation of substances that promote vasodilation, such as nitric oxide (NO), and permeability, such as VEGF [22,23]. The ensuing processes involve the disassembly of the vessel wall and subsequent degradation of the basement membrane and the extracellular matrix (ECM). These processes are predominantly mediated by angiopoietin (Ang)-2 and matrix metalloproteinases (MMPs), which are found in the endothelial cells of existing blood vessels. Ang-2 induces the detachment of smooth muscle cells and its associated basement membrane, thereby relieving inter-endothelial cell contacts. Interestingly, Ang-1 has profoundly the opposite effect, contributing to the stabilization and maturation of vessels [24]. MMPs, which are secreted by endothelial cells, stromal cells or in the case of tumorigenic angiogenesis, tumor cells themselves, degrade the capillary basement membrane and if necessary, induce the detachment of the pericytes that surround the capillary [21]. They are thought to not only provide space for migration, but also to release growth factors like VEGF and basic fibroblast growth factor (bFGF), which are normally

sequestered in the matrix. Other proteases involved in the ECM degradation process include the serine proteases, tissue plasminogen activator (tPA) and urokinase-type plasminogen activator (uPA), which convert plasminogen to plasmin [25]. Plasmin can degrade several ECM components such as fibronectin, laminin and proteoglycans, and it may possibly activate MMPs *in vivo*.

In order for endothelial cells to emigrate, the inter-endothelial cell contacts that stabilize the vessel must be modulated. Cellular adhesion molecules are important for numerous processes including cell growth, differentiation, immune-cell mediated inflammatory responses, metastases and angiogenesis. The four classes of endothelial cell adhesion molecules are integrins, cadherins, selectins and members of the immunoglobin superfamily. All have been implicated in the angiogenic process, either through observations of coincident events or through direct association [26].

Once a provisional scaffold has been established on which endothelial cells can migrate, small groups of pioneering endothelial cells negotiate the new pathway to the interstitium [20]. They are closely followed by proliferating endothelial cells that are stimulated to divide by number angiogenic inducers, some of which are released from the degraded ECM. These proliferating endothelial cells begin to organize into hollow tubes that eventually mature into a functional blood vessel [20,22,23,27].

1.4.2. Microcirculatory Assays

Chronic Transparent Chamber Assay: The rabbit ear chamber was initially developed to study wound healing [28]. The transparent chamber assay has since been used in the hamster cheek pouch for diffusion studies [29], and the dorsal skinfold window chamber was later introduced into mice to study tumor angiogenesis [30,31]. The advantage of the rabbit ear over the hamster cheek pouch and the dorsal skinfold is that the rabbit ear is thinner and more conducive to optical transillumination imaging. However, the rabbit ear and hamster cheek sites are not immunodeficient, and therefore, interrogation of tumor angiogenesis is possible only with the dorsal skinfold preparation. Cranial windows are a form of chronic transparent chamber, but they require epi-illumination and administration of contrast agents (e.g. chromophores) for inspection of the circulation. Despite this disadvantage (and the fact that it is not an immunodeficient preparation), it lasts longer in animals [32] and it permits investigation of the brain microvasculature [33]. There are limitations to the chronic transparent chamber assay, however. In comparison to other preparations, it is technically challenging and time-consuming, and any observed angiogenic effects may not initially be deconvolved from inflammation and the process of wound healing [34].

Tissue Flaps & CAM Assays: For the hamster cheek pouch, rat cremaster muscle [35] and rabbit mesentery [36] preparations, the skin above the tissue of interest is separated from the underlying fascia followed by a transplantation of the cells or pellet containing the angiogenic agent into the area. Following the necessary amount of time for that particular experiment, the skin flap is “everted” again, the degree of angiogenesis is evaluated, and the skin flap is replaced and sutured for protection until the next observation. The disadvantage

of this approach is that the eversion is traumatic, potentially confounding observations of angiogenesis [37].

The chick chorioallantoic membrane (CAM) assay is perhaps the most commonly used angiogenic assay because it is relatively inexpensive [38,39]. In the explant preparation, the entire egg contents are placed into a culture dish after a 72 hour incubation period (other preparations keep the shell and shell membrane intact except for an opening through which agents are applied). Stimulation of the system with angiogenic agents (contained in grafts, sponges, filters, or sustained-release membranes) over a span of several days can be visualized throughout the development of the embryo. Of course, a major limitation is that the cells must originate from the chicken (Gallus gallus).

In Situ Assays: The advantage of the *in situ* assay is that it can be used in rabbits, rats and mice. This system consists of a pocket in the cornea distal to the limbus. When angiogenesis-activators are placed in the pocket, peripheral limbal vascularization is stimulated [40]. The limitations of this assay are that the cornea is otherwise avascular, and physiological angiogenesis does not typically occur in avascular regions. Furthermore, in long-term observation studies, sustained release formulations can induce inflammatory reactions [41].

1.4.3. Matrix Implant Assays

Matrigel Assay: Matrigel® (BD Biosciences) is a solubule basement membrane preparation extracted from EHS mouse sarcoma cells. A Matrigel plug is created when Matrigel is injected into subcutaneous tissue where it solidifies [42]. Specific growth factors can be suspended in the liquid Matrigel which, when implanted, induce angiogenesis [43]. Disadvantages to this system include its low reproducibility and the undefined composition of Matrigel. Injection of identical amounts of the liquid Matrigel rarely forms the 3-dimensional scaffold in exactly the same way.

1.4.4. *Ex Vivo* Assays—*Ex vivo*** assays involve light or electron microscopy or histological examination of excised tissue. Light or electron microscopy involves casting, and histological examination can be done by staining for endothelial cells or perfusing the network intravascular contrast agents (e.g. colloidal carbon, radioactively labeled red blood cells (RBCs) and biotinylated high-molecular weight contrast agents) [44,45,46,47,48]. The main disadvantages of this technique are that it is invasive, and it cannot be done in the same tissue serially over time, for example, before and after stimulation with angiogenesis inducers or inhibitors.

However, an important and compelling argument for use of *ex vivo* assays is that it is currently the only method by which to analyze angiogenesis in humans. A clinical method for noninvasively observing, evaluating or assessing angiogenesis in humans will most likely come in the form of imaging techniques such as Positron Emission Tomography (PET), Single-Photon Emission Computed Tomography (SPECT), Computed Tomography (CT), Doppler ultrasound, Dynamic Contrast-Enhanced Magnetic Resonance Imaging (DCE-MRI) and optical methods, discussed below.

1.5 Tumor angiogenesis

Pathological conditions that involve uncontrolled angiogenesis include rheumatoid arthritis [49], diabetic retinopathy [50], psoriasis [51], chronic inflammation [52], and tumor growth and metastases [27,53,54]. Tumorigenic angiogenesis is a requirement for tumor growth beyond the clinically detectable size of 1–2 mm^3 [55], making it an acquired capability that is shared by most types of the invasive human tumors [15,56]. It is critical to the growth and metastases of malignant tumors, and with increasing clinical observations and subsequent investigation of tumor blood vessels, more and more evidence points to correlations between highly vascularized solid tumors (i.e. a high intratumoral microvessel density) and poor prognosis (i.e. increased incidence of metastases and reduced patient survival) [57,58]. Thus, robust measures of tumor angiogenesis will serve as potential endpoints for targeted therapies.

Tumor blood vessel permeability is an area of intense research because physiological angiogenesis and tumorigenic angiogenesis are significantly different, particularly in the context of mechanical features and the regulation of chemical mediators. Physiological angiogenesis is meticulously regulated, and new vessel growth is carefully initiated or inhibited depending on the metabolic needs of the tissue. Tumor angiogenesis is dysregulated and exacerbates competition for limited resources amongst actively proliferating tumor cells [27,59]. Tumor vessels themselves exhibit vast irregularities when compared to normal vessel characteristics [56]. Early reaction-diffusion models characterized oxygen diffusion distances to be less than 150 μm from a vessel (i.e. the Krogh cylinder) [60]. As the tumor grows beyond these life-sustaining limits, the tumor is denuded of important nutrients, such as oxygen and glucose. Carcinomas *in situ*, which are encapsulated by a basement membrane, are physically separated from vessels [59]. These avascular tumors may stay dormant and undetected for years. Once they escape basement membrane encapsulation, they may induce the formation of a customized vasculature, providing the necessary capability for tissue invasion and metastases. This evolution from avascularity to incipient neovascularization depends on the counterbalance between the inhibitory and excitatory mediators of angiogenesis in the tumor's armamentarium. Imbalances of angiogenic mediators like VEGF and the angiopoietins may contribute to the excessive branching and shunting, which paradoxically results in even more hypoxia and acidosis. The excessive leakiness or hyperpermeability of tumor vessels is in part attributed to cytokines and angiogenic factors, which presumably alter the dynamic microvessel wall [56].

1.6 Using Imaging to Estimate Microvascular Permeability

This review is focused on the measurement of microvessel hemodynamics. Of particular interest is microvascular permeability, particularly in the context of the abnormal tumor microvascular network. Flux of a tracer across the endothelium is a complex system of exchange between the vascular and extravascular space dependent on oncotic and hydraulic pressure, active and passive transport and vessel surface area. The microvessel membrane is a fluid, dynamic machine, whereas the watery membrane described in the original Kety diffusion models assumed a plane of homogenous porosity, a significant limitation to obtaining a true estimate of permeability. There is no consensus among the imaging

community regarding what measured permeability veritably represents. In truth, imaging offers only an estimation of permeability, or an ‘effective’ permeability based on tracer enhancement kinetics (discussed in more detail in later sections), and thus, on this macroscopic level, the rate of enhancement is related to microvascular permeability through complex kinetic models. However, it is prudent to consider that there are many other factors affecting this process that are involuted into the assumptions of these tracer kinetic models.

Although a measure of effective permeability can be theoretically derived from quantitative imaging data, there has been limited progress in the development of *in vivo* imaging systems that can truly quantify this parameter. The nuclear medicine modalities such as PET and SPECT, as well as CT have dynamic tracer imaging capabilities for measuring tumor microvessel permeability, but exposure to continuous radiation limits their use in longitudinal studies and acquisition of images with high spatio-temporal resolution. Optical measurements are also robust in terms of quantitation but a major limitation is a lack of penetration depth, which is a significant impediment to clinical translation. Ultrasound is noninvasive and nonionizing and is clinically ubiquitious, but it only measures perfusion (not permeability) moderately well and suffers from low signal to noise ratio, poor dynamic range and low frequency resolution. DCE-MRI is also nonionizing, but poor reproducibility in both image acquisition and analysis across image sites and institutions reduces confidence levels. This review will present the basic methodology, strengths and weaknesses for each of these systems with respect to their ability to produce reliable and robust measures of effective tumor vascular permeability.

2 Imaging the Tumor Microvasculature

2.1 Introduction: Survey of Methods

Useful imaging systems have been developed to monitor angiogenesis and the microvasculature *in vivo*, including PET and SPECT, CT, Doppler ultrasound, optical imaging methods and DCE-MRI. The following table is a brief overview of the overall coverage, resolution and sensitivity associated with each imaging system. Each system has strengths and limitations in terms of their ability to measure microvascular hemodynamics, all of which will be reviewed in their respective sections.

2.2 Table: Comparison of Imaging Systems

Modality	Contrast Agent/Tracer	Penetration	Resolution	Sensitivity
PET	$H_2{}^{15}O$, $C^{15}O_2$,^{11}C	Whole Body	1–3 mm	10^{-11}–10^{-12} mol/L
SPECT	IMP, ^{99m}Tc-Alb sesamibii	Whole Body	0.5–5 mm	10^{-10}–10^{-11} mol/L
CT	Iodinated Tracers	Whole Body	0.05–0.8 mm	Not well characterized
Ultrasound	Microbubbles	9 cm @ 7 MHz	0.1 mm	Single bubbles
MRI	Gd-DTPA	Whole Body	0.1–1.5 mm	10^{-3}–10^{-5} mol/L
Optical Imaging	Fluorochromes	<1 cm	0.2–1.0 μm	10^{-9}–10^{-12} mol/L

2.3 Measurement of Hemodynamics with Nuclear Medicine (PET/SPECT)

Positron emission tomography is based on the approximate collinearity of two photons simultaneously emitted by the annihilation of a positron and electron. The resolution of PET is limited by uncertainties arising from the approximation of collinearity and annihilation position due to individual positron ranges [61].

Generally, PET measures of tumor perfusion have used (^{15}O)-labeled radiotracers. An important study compared steady-state and dynamic methods for determining blood flow in 22 patients with liver metastases [62]. The steady-state method required inhalation of [^{15}C]-O_2 and the dynamic method required an intravenous bolus injection of [^{15}O]-H_2O. Although both methods produced similar quantification of blood flow, the correlation between methods was low. The dynamic method was superior in its ability to quantify blood flow in hepatic metastases. This method also delivered close correlations to angiographic data, demonstrating that the degree of vascularization, as determined by PET, can reliably differentiate between tumor grades.

A requirement for quantification of perfusion using dynamic methods is an accurate determination of an arterial input function, which can be obtained noninvasively in a purely arterial region of interest, such as the aorta [63,64]. This also allows for determination of the volume of distribution parameter (V_d), which is the proportion of exchanging water space between tissue compartment and vascular compartments. With these corrections, the coefficients of variation can be minimized. Using ^{15}O-labeled carbon dioxide ([^{15}O]-CO_2), intra-patient coefficients of variation for measurement of flow and V_d were 11% and 6%, respectively [65].

2.3.1. Response to Antivascular Therapy—One of the first randomized clinical trials to use ^{15}O-labeled tracers measured vascular hemodynamics in a Phase I dose-escalation study of combrestatin A4 phosphate (CA4P), an antivascular therapy [66]. In 13 patients with a variety of solid tumors, significant reductions in perfusion were observed as measured by [^{15}O]-H_2O 30 minutes and 24 hours post-treatment. Significant reductions in blood volume could be measured by ^{15}O-labeled carbon monoxide ([^{15}O]-CO), which binds to hemoglobin and is thus intravascular. These also show similar reductions within 30 minutes of CA4P, yet these were followed by a vascular recovery 24 hours later. In a Phase II clinical trial, 12 patients with solid primary or metastatic renal tumors were evaluated with [^{15}O]-H_2O, and [^{15}O]-CO in response to the antiangiogenic therapy, razoxane [67]. Perfusion and blood volume data were obtained from only six of the total enrolled patients. Although the mean post-treatment perfusion was lower than pre-treatment, these were not statistically significant. For this drug, there was virtually no change in blood volume pre- versus post-treatment. There was also no correlation found between pre-treatment perfusion and tumor size (as estimated by CT), nor was there a correlation found between perfusion and patient response or survival. Another study investigated the effects of SU5416, a small molecule inhibitor of the tyrosine kinase domain of the VEGF receptor, Flk-1, in renal cell carcinoma patients [68]. Following treatment, no patients had a clinical response, but 15 of 23 patients demonstrated stable disease. In patients with available data, perfusion (as determined by [^{15}O]-H_2O) and metabolism (as determined by ^{18}FDG) decreased or

minimally changed in patients with stable disease and increased in a patient with progressive disease.

2.3.2. Response to Cytotoxic Therapy—PET-measured perfusion and blood volume changes following treatment with cytotoxic therapy were quantified in 19 patients bearing stage II or III breast tumors [69]. This study found no correlation between response to therapy and perfusion using [^{15}O]-H_2O, but found a positive correlation in total blood volume as measured by ^{11}C-labeled carbon monoxide ([^{11}C]-CO). Another study involved investigation of improved delivery of a cytotoxic therapy, 5-fluorouracil (5-FU), using a vasopressor (nicotinamide) concomitant with carbogen inhalation. The hypothesis was that such a treatment would enhance the delivery of 5-fluorouracil by increasing tumor blood flow [70]. Patients with colorectal metastases were intravenously administered [^{15}O]-H_2O, imaged for 10 minutes, then given [^{18}F]5-FU intravenously and imaged for another 90 minutes. Nicotinamide and carbogen were administered only on the second imaging session, concurrent with the second cycle of chemotherapy. Both tumor perfusion and delivery of 5-FU to the tumor were observed to increase significantly in response to nicotinamide/carbogen.

Finally, an interesting study was designed to examine the relationship between hypoxia and perfusion in 11 patients with various brain tumors [71]. ^{18}F-fluoromisonidazole (^{18}F-FMISO) is a nitroimidazole derivative that is trapped by hypoxic cells and this was injected following measurement of [^{15}O]-H_2O distributions to evaluate perfusion. There was a positive correlation between tumor perfusion and ^{18}F-FMISO tumor uptake within the first 5 minutes of the ^{18}F-FMISO injection, probably reflecting delivery. At later time points, ^{18}F-FMISO uptake occurred in areas that were not perfused (as measured by [^{15}O]-H_2O), suggesting that hypoxia developed in areas with poor perfusion.

Single photon emission computed tomography (SPECT) is routinely used to measure perfusion in the clinic. Although it has lower sensitivity compared to PET, the spatial resolution is theoretically higher, as it is not dependent on positron annihilation [61]. Dynamic SPECT is an improvement to conventional SPECT, offering faster detector rotation, high-resolution, high-sensitivity dynamic and static collimators and filtered back-projection reconstruction. Dynamic SPECT can be used to measure cerebral blood vessel dynamics [72]. SPECT of N-isopropyl-p[^{123}I]-iodoamphetamine (IMP) has been used to positively differentiate between blood flow in brain tumors and normal gray matter, indicating a disruption in tumor-associated vessel permeability [73]. The intravascular agents, Technetium-99m-labeled albumin (^{99m}Tc-HSA), has been used to measure permeability in patients with hepatic tumors, and perfusion was shown to increase compared to normal tissue following epinephrine infusion in 67% of the patients [74]. Another study demonstrated that hepatic arterial perfusion scintigraphy (HAPS) using ^{99m}Tc-HSA was useful in assessment of catheter placement and perfusion, changes in perfusion during chemotherapy and arteriovenous shunting to the lung [75]. Thallium-201 (^{201}TlCl) chloride and ^{99m}Tc-diethylenetriaminepenta-acetic acid labeled HSA (^{99m}Tc-HSA-D) were used to assess tumor viability and tumor vascular permeability, respectively, in 17 patients. Within one month post-radiotherapy, both systems delivered values that were significantly reduced compared to pre-therapy values [76]. In another study, patients with various soft tissue and

bone tumors were imaged using ^{99m}Tc labeled hexakis-2-methoxyisobutylisonitrile (^{99m}Tc-MIBI) [77]. The perfusion index was derived by dividing the peak count of the arterial phase by that of the contralateral tissue, and the MIBI-uptake ratio was derived by dividing the count density of the tumor by that of the contralateral tissue. Both the perfusion index and the MIBI-uptake ratio of benign lesions were significantly lower compared to malignant lesions. Setting a threshold cutoff for the perfusion index of 10.0, sensitivity, specificity, accuracy, PPV and NPV values of 40%, 100%, 71%, 100% and 64% respectively, were possible. This cutoff was not dependent on tumor size. Though many studies have used ^{99m}Tc-MIBI to evaluate tumor perfusion, they have primarily used planar scintigraphy to evaluate the perfusion characteristics. For example, patients with various cancers have been evaluated with ^{99m}Tc-hexamethylpropylenamineoxime (HMPAO), and a hypoxia-related tracer, iodoazomycin arabinoside (IAZA) labeled with ^{123}I [78]. In general, an inverse correlation between perfusion and uptake of IAZA was observed in all tumor types except for glioblastoma multiforme.

2.3.3. Kinetic Modeling of PET/SPECT Data—Radioisotope measurements of tracer distribution into tissues are well-characterized. The relationship between blood flow and tracer clearance was originally described by Fick in 1870. In 1978, Ohno et al. modified the Fick equations of tracer diffusion to describe the distribution of ^{14}C-labeled-low molecular weight compounds [79]. In this formalism, the plasma concentration can be represented as a sum of decaying exponentials:

$$C_p(t)=\sum_{i=1}^{n} A_1 e^{-m_i t}. \quad \text{Equation 6}$$

When blood flow (F) is much more than the permeability surface area product (PS), transport across the capillary is independent of flow. If, in addition, the vascular fraction of the tracer can be assumed to be negligible, the tissue tracer uptake per unit gram of tissue can be expressed as:

$$\frac{dC_t}{dt}=PS\left(C_P-\frac{C_t}{v_e}\right), \quad \text{Equation 7}$$

where C_t is the tissue concentration, v_e is the extracellular extravascular space per unit volume of tissue and $C_e=C_t/v_e$. Ohno et al. did not include the tissue density (ρ) in their equations, stating that brain specific gravity (a dimensionless quantity) was approximately 1.0. Accounting for tissue density and solving this differential equation leads to:

$$C_t(t)=PS\rho\sum_{i=1}^{n}\frac{A_1}{m_i-(PS\rho/v_e)}e^{-(PS\rho/v_e)t}-e^{-m_i t}, \quad \text{Equation 8}$$

and early in the time course, when flow of tracer is unidirectionally moving out of blood into the tissue,

$$PS = \frac{C_t}{\rho \int_0^t C_p(t')dt'}. \quad \text{Equation 9}$$

Essentially, tracer cleared by the tissue over time is a function of the perfusion of the tracer and the extraction of the tracer.

2.3.4. Table: Measurement of Hemodynamics with PET/SPECT

Tracer	System	Parameter Measured	Results	Reference
PET ($[^{15}O]$-H_2O, $[^{15}C]$-CO_2)	Liver metastases	Perfusion	Comparing dynamic versus steady state methods, differentiation between tumor grades	[62]
PET ($[^{15}O]$-H_2O)	Breast tumors	Perfusion and distribution volume	Evaluated non-invasive AIF measurement and obtained better estimations of distribution volume	[63]
PET ($[^{15}O]$-H_2O, ^{18}FDG)	NSCLC	Perfusion and tumor localization	Large interpatient variations, inaccurate estimation of perfusion	[64]
PET ($[^{15}O]$-H_2O, $[^{15}C]$-CO)	Solid tumors	Perfusion and blood volume	Phase I dose-escalation study, perfusion and blood volume decreases in response to CA4P	[66]
PET ($[^{15}O]$-H_2O, $[^{15}C]$-CO)	Solid/metastatic renal tumors	Perfusion and blood volume	Phase II study, insignificant decreases in perfusion and BV in response to razoxane	[67]
PET ($[^{15}O]$-H_2O)	Renal tumors	Perfusion and metabolism	Perfusion decreases in patients with stable disease in response to SU5416	[68]

Tracer	System	Parameter Measured	Results	Reference
PET ([^{15}O]-H_2O, [^{11}C]-CO)	Breast tumors	Perfusion and blood volume	No significant association between perfusion and response to treatment; insignificant increase in blood volume in non-responding tumors	[69]
PET ([^{15}O]-H_2O)	Colorectal metastases	Perfusion	Enhanced delivery of 5-FU via carbogen and nicotinamide, significant increase in perfusion post-treatment	[70]
PET ([^{15}O]-H_2O, ^{18}F-FMISO)	Brain tumors	Perfusion and hypoxia	Early uptake correlations between perfusion and hypoxia, no late uptake correlations	[71]
SPECT (IMP)	Brain tumors	Perfusion	Differentiation between perfusion of tumor and perfusion of normal tissue	[73]
SPECT (^{99m}Tc- HSA)	Liver tumors	Perfusion	Increased perfusion in tumor following infusion of epinephrine	[74]
SPECT (^{201}TICI, ^{99m}Tc-HSA-D)	Brain metastases	Permeability and viability	Significant post-treatment reductions in permeability and viability	[76]
SPECT (^{99m}Tc- MIBI)	Soft tissue and bone tumors	Perfusion and MIBI uptake ratio	Perfusion and MIBI uptake ratio lower in benign versus malignant tumors, achievable predictive value of these parameters	[77]
SPECT (^{99m}Tc- HMPAO, IAZA)	SCLC, GM, brain metastases, prostate and head and neck tumors	Perfusion and hypoxia	Inverse correlation between perfusion and uptake of IAZA in all tumors but GM tumors	[78]

2.4 Measurement of Hemodynamics with Computed Tomography

In X-ray computed tomography (CT), tissue contrast is based on variable attenuation coefficients (Hounsfield units) of the object absorbing the X-rays [61]. Hemodynamic parameters may be extracted from dynamic changes in X-ray attenuation caused by the intravenous injection of a contrast agent. Perfusion CT data can deliver quantitative hemodynamic information, such as blood volume, blood flow, permeability surface-area product and mean transit time (MTT). An example includes diagnostic differentiation of rectal cancers from normal tissue based on elevated blood flow and attenuated MTT in the tumor and measurable post-treatment changes in blood flow and MTT [80]. Notably, it was even possible with this small data set to make general conclusions about the predictive value of this imaging system for patient response, as it appeared that a higher pre-therapy perfusion index and shorter MTT was associated with a poorer therapeutic outcome.

In a larger study, 77 patients with primary oropharyngeal and oral carcinoma, questionable recurrent disease and suspected metastatic lymph nodes were evaluated with perfusion CT [81]. In this study, a deconvolution model with a 2 compartment analysis was applied for capillary permeability-surface area product (PS) measurements. Other parametric maps were obtained for blood flow, blood volume and MTT. All parameters except for MTT were significantly higher in tumors compared to normal tissue. MTT was significantly lower than that of normal tissue. Furthermore, the perfusion measurements sufficiently differentiated between primary and recurrent tumors. In head and neck squamous cell carcinomas, perfusion CT was able to reliably and significantly differentiate between tumor and normal tissue [82]. Parametric maps of blood flow, blood volume and permeability demonstrated significantly larger values compared to normal tissue and the mean transit time was significantly attenuated compared to normal tissue. In hepatic metastases, median values of arterial perfusion were greater in the metastatic tissue compared to adjacent normal tissue [83]. An advantage of CT is the excellent spatial resolution, allowing observation of microenvironmental heterogeneities. In just under half of the patients evaluated, peripheral perfusion of the tissue surrounding the tumor was higher than the ROI containing only tumor, suggesting that neovascularization is occurring well beyond the margin of the tumor. In some patients, low perfusion was observed in the center of the tumor. Notably, there were statistically significant correlations established between patient survival and perfusion of the metastatic lesions and adjacent liver tissue; i.e. a higher perfusion index was correlated to longer survival times ($p<0.05$, $r = 0.69$). In a separate study conducted on 21 patients with lymphoma, median perfusion values were higher in patients with active, high or intermediate lymphoma, and perfusion values below 0.2 ml/min/ml indicated inactive disease [84]. In this study, values of permeability did not produce information allowing for the differentiation between grades or lymphoma activity status.

A small study was conducted to assess the reproducibility of CT measured hemodynamics within a Phase IB clinical trial of combrestatin A4 phosphate in 10 patients with inoperable non-small lung cell cancer (NSCLC) [85]. Parametric maps of permeability and blood volume were derived based on a Patlak analysis, and both parameters demonstrated good agreement between studies, with a CV of 9.49% and 26.31% for permeability and blood volume, respectively. In this study, an increase or decrease in tumor permeability over 8.3%

would have been significant. Goh *et. al.* assessed intra- and inter-observer reproducibility for blood volume, blood flow, mean transit time and permeability from dynamic CT in patients with colorectal carcinoma [86]. The correlation coefficients for the inter-observer variability ranged from 0.8 to 0.89 for all perfusion parameters, and the intra-observer correlation coefficients ranged from 0.86 to 0.98, indicating excellent agreement in both cases. The same group also found that when imaging abdominal cancers, acquisition times under 45 minutes would result in significant degradation of permeability measurements but not blood flow, blood volume or meant transit time [87]. Dynamic CT has also been used to assess patient response to bevacizumab [88] and for a Phase I dose finding study of MEDI-522, a humanized anti-body to the $\alpha_v\beta_3$ integrin [89]. In this latter study, of all the measured parameters (blood flow, blood volume, permeability surface area product and MTT), only the MTT demonstrated a significant change with increasing dose of MEDI-522.

2.4.1. Kinetic Modeling of Perfusion CT Data—A widely used model of perfusion CT kinetic parameters which also accounts for diffusive resistances and concentration gradients (i.e. a distributed parameter model) was described by Johnson et al. [90] and later modified for a solution with an adiabatic approximation by St. Lawrence et al. [91]. According to the model, a contrast agent enters the intravascular space and is described as having a concentration, $C_b(x,t)$, which decreases from the arterial inflow of the capillary, $C_a(t)$, to the venous outflow, $C_v(t)$. $C_e(t)$ represents the change in the contrast agent concentration in the extravascular, extracellular space over time, V_e represents the interstitial volume, V_b represents the blood volume, F represents the flow rate and PS represents the permeability-surface area product. The convective and diffusive transport of the contrast agent is represented by [80]:

$$\frac{\partial C_b(x,t)}{\partial t}+\frac{FL}{V_b}\cdot\frac{\partial C_b(x,t)}{\partial x}+\frac{PS}{V_b}[C_b(x,t)-C_e(t)]=0, \quad \text{Equation 10}$$

and the evolution of the contrast agent concentration in the interstitial compartment is described by:

$$V_e\frac{dC_e(t)}{dt}=\frac{PS}{L}\int_0^L[C_b(x,t)-C_e(t)]dx. \quad \text{Equation 11}$$

Using these equations to model enhancement kinetics, four vascular parameters, vascular permeability, vascular blood volume, MTT and blood flow, can be estimated simultaneously [80].

2.4.2. Table: Measurement of Hemodynamics with CT

Tracer	System	Parameters Measured	Results	Reference
Iopamidol (Isovue)	Rectal tumors	Perfusion and mean transit time	Decreased perfusion and increased mean transit time post-treatment; high perfusion index and short MTT index	[80]

Tracer	System	Parameters Measured	Results	Reference
			poor response to therapy.	
Iomeron (Iomeprol)	Oropharyngeal and oral tumors	Permeability, blood flow, volume and mean transit time	All parameters elevated in tumors compared to normal tissue except for low mean transit times; differentiation between primary and recurrent tumors based on blood flow	[81]
Iodinated contrast agent	Head and neck tumors	Permeability, blood flow, blood volume and mean transit time	All parameters were significantly different in tumors compared to normal tissue	[82]
Iopamidol (Isovue 300)	Hepatic metastases	Perfusion	Perfusion elevated in metastases compared to contralateral tissue; significant correlation between survival and perfusion of metastasis (higher perfusion, increased survival)	[83]
Iopamidol (Isovue 300)	Lymphoma	Perfusion and permeability	Perfusion correlated well with grade and activity but permeability did not reliably differentiate between grade or activity	[84]
Iobitridol (Xenetix 30)	Non-small cell lung cancer	Perfusion, permeability and blood volume	Reproducibility of whole tumor perfusion both parameters was acceptable	[85]
Iopamidol (Niopam 340)	Colorectal tumors	Blood volume, blood flow, mean transit time and permeability	Correlation coefficients for interobserver variability and intraobserver variability indicated excellent agreement in both cases	[86]
Iopamidol (Niopam 340)	Colorectal tumors	Perfusion	Early changes in perfusion of tumors responding to bevacizumab demonstrated	[88]
Iodinated contrast agent	Advanced solid tumors refractory to therapy	Blood flow, blood volume, permeability and mean transit time	Phase I dose-escalation study of MEDI-522; only mean transit time demonstrated significant changes post- treatment	[89]

2.5 Measurement of Hemodynamics with Ultrasound

Medical ultrasonography is based on the pulse-echo and back-scattered echo waveforms. A transducer which converts electric power to acoustic power is used to transmit short and relatively broadband pulses through the tissue, which are attenuated at tissue interfaces due to absorption and scattering. The pressure from the backscattered signal is collected by the same or a second phase-sensitive transducer, and the output voltage is a radiofrequency trace

which is recorded as a function of the acoustical travel time in the tissue. Because the trace is an amplitude-modulated display of the backscattered waveform, it is referred to as an A-mode display or A-scan. The ultrasound image is created by converting the A-mode display into a brightness mode display along a vertical axis. The horizontal profile of waveform spikes is now converted into a vertical series of bright dots. Moving the transducer along the specimen will create a 2 dimensional image of bright dots in the same manner, hence the term B-mode display. The fundamental limit to resolution in ultrasonography is the frequency-dependent attenuation. Higher transducer frequencies offer better resolution but greater tissue attenuation. Thus, any improvement in lateral resolution implies a loss in depth of penetration.

There are several different ultrasonic approaches designed specifically to measure blood flow including transit time, continuous-wave Doppler, pulsed and color Doppler and power Doppler flowmeters. Transit-time flowmeters operate under the phase-shift principle and utilize two transducers to measure blood flow velocity. However, the transit-time flowmeter is infrequently used for routine estimation of flow because invasive surgery is required to expose the vessel. Unlike transit-time flowmeter, the continuous-wave (CW) Doppler flowmeter requires particulate matter, such as blood cells, for scattering. In CW Doppler ultrasound, red blood cells are considered reflecting targets, and when those targets recede from a stationary sound source (transducer), the frequency of the received sound is shifted proportionally to their velocity relative to the transmitter and receiver [92]. The Doppler frequency shift is expressed as:

$$f_d = \frac{2 f_0 u \cos\theta}{c}, \quad \text{Equation 12}$$

where f_0 is the source frequency, c is the velocity of sound, u is the target velocity and θ is the angle between acoustic transmission and the long axis of the blood vessel. Pulsed Doppler ultrasound is the most broadly applied ultrasound technique. In this, the delay between a brief transmitted wave and its reception is directly proportional to distance, so a complete plot of reflections across the blood vessel can plotted, generating a velocity profile based on Doppler shifts. The tradeoff for high resolution (short pulses) is a better signal-to-noise ratio (long pulses). Furthermore, since the pulse system is broadband, it is inherently more sensitive to electronic noise, resulting in low dynamic range and rendering it less capable of detecting small volumes of blood. Color Doppler is termed as such because pulse Doppler-derived velocity information is color mapped onto grayscale ultrasound images. The most common estimation of the velocities uses consecutive transmit pulses at fixed depths to find the phase difference between received echoes. Color Doppler has been successfully used to evaluate abnormal perfusion profiles in liver [93], ovarian [94], breast [47,48] and prostate carcinomas [46]. In a newer modification, called Power Doppler, color is encoded based on the integrated power of the Doppler signal rather than the mean Doppler frequency shift [95]. The advantages of power Doppler over color Doppler include a lower noise variance and ability to spectrally encode noise in order to differentiate it from information signal. Other advantages include angle independence and immunity to aliasing because the power remains the same as a function of phase shift, and depth-compensation [92].

Contrast-enhanced ultrasound has become increasingly popular for measuring perfusion. The first ultrasound contrast agent was reported in 1968 [96]. Since then, the explosion of microbubble research has made ultrasonography a useful contrast-enhanced clinical imaging utility. Microbubbles are comprised of an outer shell, generally composed of lipids, proteins, or polymers, and a gas inner core filled with air, perfluorocarbon, sulfur hexafluoride or nitrogen [97]. Microbubbles expand and contract due to pressure from the acoustical transmit pulse, and the primary mode of echogenicity is the impedance mismatch between the microbubble-blood interface, making them significantly more echogenic than normal tissue. However, there are many other manifestations of microbubble contrast including increased scattering cross-section, nonlinearities from increased acoustic pressure that give rise to unique harmonics, and transient, non-linear signal emission from bubble disruption (a.k.a. cavitation).

Although it is not routine, contrast-enhanced ultrasound is used to measure hemodynamics in human tumors. In recurrent breast cancer patients, contrast agent uptake after RF ablation therapy has been used to successfully predict responders, indicating a strong ability to estimate tumor vascularity [98]. In solid breast tumors, contrast enhanced ultrasound has also been used to provide a measure of solid breast tumor vascularity as compared to histological analysis of vascularity [99]. Compared to conventional B-mode scanning and CT, contrast-enhanced ultrasound sensitively differentiated patients with metastatic liver lesions (~95%, compared to 50% and 59% for B-mode scanning and CT, respectively) [100]. Contrast-enhanced ultrasound is capable of differentiating between non-functional islet tumors (often misdiagnosed as ductal adenocarcinoma) from pancreatic carcinoma. The differential diagnosis criteria included age, size, margin, level of vascularity and enhancement timing [101]. A notable quantitative study conducted on untreatable hepatocellular carcinomas showed that post-treatment with thalidomide, the percent blood volume, average red blood cell velocity and the product of the two, perfusion, all decreased significantly following therapy, even in patients followed out to 2-years [102].

2.5.1. Modeling of Perfusion Ultrasound Data—Hertz was the first to provide the idea of estimating perfusion using continuous wave Doppler ultrasound [103], and this was closely followed by Dymling [104] with a mathematical estimation of perfusion based on the measured Doppler power spectrum. Perfusion was expressed as follows:

$$P=\frac{Q_c}{V_s}\approx n_c E\left\{v_c\right\}, \quad \text{Equation 13}$$

where Q_c is total capillary flow, V_s is the sample volume of tissue, n_c is the number of capillaries per unit volume tissue and $E\{v_c\}$ is the average blood velocity in the capillaries. To establish the proportionality between perfusion and a Doppler-derived measurement, the assumption was made that red blood cells were the primary, isotropic scattering source:

$$\int_0^\infty fS(f)df\approx N_0 E\left\{v_c\right\}. \quad \text{Equation 14}$$

Such an expression relates the mean number of red blood cells in some volume of interest and their mean speed along the z-axis to the first moment of the Doppler power spectrum.

This expression can be used to estimate velocity using any of the above ultrasound techniques, but the modern flow mapping techniques estimate perfusion by quantifying the density of colored pixels or number of visible vessels in a given region of interest relative to normal tissue.

An interesting method to estimate perfusion was demonstrated in myocardium using contrast-enhanced ultrasound and selective high-power pulses to destroy microbubbles and observe the inflow of unaffected microbubbles during a continuous infusion. The so-called 'refilling' signal reflected the mean myocardial microbubble velocity. The asymptotic maximum was related to fractional vascular volume, and the product of the two parameters was related to perfusion [102,105]. This approach has yet to be used in cancers, although focused ultrasonic cavitation of microbubbles has been identified as a promising technique for imaging and delivery of therapies [106,107,108,109].

2.5.2. Table: Measurement of Hemodynamics with Ultrasound

Tracer	System	Parameter Measured	Results	Reference
Sonovue® (microbubbles)	Power Doppler US	Percent intratumor contrast agent uptake	Following RF ablation therapy, DUPC accurately estimated degree of vascularization in 80% of cases	[98]
Levovist® (microbubbles)	CEUS	Tumor vascularity	Post-contrast vascularity correlated well with histological assessment of vascularity	[99]
Sonovue® (microbubbles)	CEUS, conventional B-mode US, spiral CT	Number of metastases	CEUS outperformed conventional US and CT in its ability to accurately detect more metastatic lesions	[100]
Sonovue® (microbubbles)	CEUS, color Doppler US	Enhancement timing & pattern (related to vascularity)	Accurate differentiation between nonfunctional islet tumors and pancreatic carcinoma	[101]
Sonovue® (microbubbles)	CEUS	Percent blood volume fraction, RBC velocity & perfusion	Post-treatment changes in these parameters following treatment with thalidomide	[102]

2.6 Measurement of Hemodynamics with Optical Imaging

"Optical imaging" describes a broad range of techniques. Methods specifically designed for *in vivo* imaging include photo-luminescence (*fluorescence*) and chemi-luminescence (commonly referred to as *bioluminescence*). An additional approach that may have clinical utility is diffuse optical (DOT) tomography. This method utilizes the diffusion equation to model propagation of light through tissue using the absorption and scattering coefficients.

A major limitation of optical imaging is the depth of penetration because scattering and absorption increase as a function of tissue depth. Thus, capturing images from outside the body is difficult. However, sophisticated optical images can be obtained by detectors

attached to endoscopes. The major advantages of optical imaging are its temporal, spatial and spectral resolution. Using reflected light and fluorescence light at a micrometer resolution (for example, confocal microscopy), cancerous cell morphology can be interrogated, and multispectral imaging with millimeter resolution can be used to interrogate general tissue morphology [110]. Optical imaging is capable of capturing real-time dynamics particularly with recent improvements in the quality of fast and highly sensitive cameras.

The advancement of fluorescence microscopy in biomedical research is partly attributed to the development of methods to conjugate proteins to fluorochromes [111,112], and partly to improvements in thin film technology and opto-electronics, which increased the sensitivity and specificity of detection of emitted fluorescent light [113]. Most filters sets are not totally efficient in eliminating damaging and unwanted UV wavelengths, so fluorescence imaging can be damaging to tissues. The primary mechanisms of damage are phototoxicity (i.e. absorption of photons by exogenous and endogenous fluorochromes) and creation of reactive oxygen species (ROS). This can be mitigated somewhat by two-photon or near-IR imaging which uses longer wavelengths for excitation. A further advantage of NIR imaging is that the range of wavelengths (700–900 nm) maximizes depth of penetration while minimizing scatter and background autofluorescence [114]. Chemi-luminescence imaging is based on the catalysis of light emission from a substrate. The most common and fully developed reporter is the luciferase enzyme which oxidizes luciferin. Light emitted from this reaction is between 530–640 nm (broad-band) [115].

In general, optical imaging of vascular permeability has been limited to pre-clinical studies. However, there are currently more than 10 ongoing clinical trials that are using optical imaging to study human tumors [116]. Fluorescence/reflectance imaging and confocal microscopy are used to detect surgical resections of non-melanoma skin cancers; non-invasive, scanning two-photon fluorescence microscopy is being used to replace the skin biopsy; optical spectroscopy is being investigated as a potential use for intraoperative margin assessment during breast cancer lumpectomy; and transillumination breast spectroscopy is being developed as breast cancer risk predictor to replace and or augment mammographic parenchymal density.

Diffuse optical tomography (DOT) is potentially useful for measuring hemodynamics. DOT propagates light through the tissue at multiple projections to yield a 3-dimensional tomographic image of deep tissue organs and, depending on the mathematical approach taken, maps of absorption, scattering, vascularization, oxygenation, and contrast agent uptake can be generated [117]. In a recent study that used DOT concurrently with dynamic contrast-enhanced MRI, the distribution of fluorescent indocyanine green (ICG) was compared to that of an MR-contrast agent, Gd-DTPA, and found that they were correlated [118].

The transillumination limitation of optical imaging can be overcome with a pre-clinical, *in vivo* chronic transparent chamber angiogenesis assay, the dorsal skinfold window chamber technique. Coupled with intravital fluorescence microscopy, this technique has provided tremendous insight into basic vessel physiology and is capable of providing quantitative

measurements of blood flow, vascular volume, permeability, vessel density, gene expression and drug delivery in animals [119]. Tozer et al. has used the window chamber model and intravital fluorescence microscopy to show combretastatin A-4 3-*O*-phosphate and nitric oxide synthase effects on vascular permeability [120].

2.6.1. Kinetic Modeling of Dynamic Optical Imaging Data—A very comprehensive study using fluorescence video microscopy to measure vascular permeability was performed in the window chamber model [121]. The derivation of vascular permeability as measured optically begins with the assumption that the relationship between number of fluorochromes (*N(t)*) in the vascular and interstitial space and the average fluorescent intensity (*I(t)*) in the vascular and interstitial space is linear:

$$I_v(t)=\frac{k_v \cdot N_v(t)}{A}, \quad \text{Equation 15}$$

$$I_i(t)=\frac{k_i \cdot N_i(t)}{A}, \quad \text{Equation 16}$$

where k_v (vascular) and k_i (interstitial) relate the number of fluorochromes in area *A* to the average light intensity in *A*.

From Fick's Law, the average permeability coefficient (*P*) is the ratio of the flux of tracer (J_s) to the product of the vessel surface area and difference between the plasma concentration (C_p) and the average interstitial concentration (C_i):

$$P=\frac{J_s}{S \cdot (C_p - C_i)}. \quad \text{Equation 17}$$

Assuming that the flux is approximately equal to the rate of accumulation of tracer in the interstitial space, and substituting C_p and C_i for parameters that account for vascular volume (V_v), tube hematocrit (H_T) and volume to surface area ratio (λ), the following equation is derived:

$$I_i(t)=\alpha \cdot \int_0^t e^{-\beta(t-\tau)} \cdot I_v(\tau) d\tau, \quad \text{Equation 18}$$

which relates the constants α and β to permeability as follows:

$$P=\alpha \cdot \left[\lambda \cdot (1-H_T) \cdot \left(\frac{k_v}{k_i}\right)\right]. \quad \text{Equation 19}$$

A complete description of the derivation is provided elsewhere [121].

2.6.2. Table: Measurement of Hemodynamics with Optical Imaging

Tracer	System	Parameter Measured	Results	Reference
ICG (indocyanine green)	DOT	Tracer distribution	Comparable distribution kinetics with Gd-DTPA (as measured by MRI)	[118]

2.7 Measurement of Hemodynamics with Magnetic Resonance Imaging

Dynamic contrast enhanced (DCE)-MRI has been used extensively to measure microvascular permeability in many human tumors, such as bone sarcomas [122], head-neck and prostate tumors [123], breast tumors [124], cerebral gliomas [125], and breast tumors [126]. DCE-MRI is a non-invasive, functional method to measure active changes in hemodynamic parameters occurring following treatment before macroscopic changes, such as decreases in tumor volume, become evident. Currently, there are at least 11 clinical trials in all four phases dedicated to the interrogation of tumors and tumor response to therapy using information derived from DCE-MRI [116]. DCE-MRI is used to experimentally characterize the tumor microvasculature by modeling the pharmacokinetics of injected contrast agents. These unique MRI contrast agents are chelated with Gadolinium and generate very large magnetic lattice fields in the immediate neighborhood of the complex, greatly shortening the T1 or longitudinal relaxation of water protons that approach the paramagnetic center. This lends to the unique contrast between tissues observed using this imaging approach. The efficiency with which a contrast medium can shorten T1 relaxation is determined by its inherent relaxivity.

2.7.1. Table: Measurement of Hemodynamics with DCE-MRI

Tracer	System	Parameter Measured	Results	Reference
GdDTPA (Magnevist)	Bone sarcoma	Permeability	Associations found between expression of VEGF and increases in permeability	[122]
GdDTPA (Magnevist)	Head & neck, prostate & brain neoplasms	Rate of uptake, k_{ep}	Demonstrated reproducibility of k_{ep}	[123]
GdDTPA (Magnevist)	Breast tumors	Permeability	Significant change in permeability pre- and post- treatment	[124]
Gadodiamide (Gd- DTPA-BMA)	Cerebral glioma	Permeability	Demonstrated reproducibility of permeability	[125]
GdDTPA (Magnevist)	Breast tumors	Exchange rates	Significant differentiation between malignant and benign tissue	[126]

2.7.2. MRI Contrast Media—The challenges remaining in the development and application of MR contrast agents are 1) to find media that are most sensitive to microvascular permeability and; 2) to quantify the values obtained from images. Generally, DCE-MRI measurements using high molecular weight contrast agents (HMWCA) are more sensitive to the transendothelial capillary permeability, while DCE-MRI measurements

using small molecular weight contrast agents (SMWCA) are more sensitive to flow. Although SMWCA are commonly used in the clinic, they rapidly extravasate in tumors and normal tissues with fenestrated or sinusoidal capillaries. Quantification of this rapid extravasation requires rapid image acquisition, at the expense of reduced spatial resolution. Furthermore, extravasation rates are flow-dominated, so SMWCA are insensitive to drug-induced changes in microvascular permeability. HMWCA do not extravasate rapidly, and measurements made using them are more sensitive to changes in microvascular permeability. Imaging performed using HMWCA can be at higher spatial resolution at the expense of temporal resolution, given the slow extravasation rates. Thus, there is an interest in developing intravascular compounds that demonstrate a large dynamic range and sensitivity to changes following interventional therapies in cancer [127]. To be clinically useful, these agents must be non-toxic and have high relaxivity, which will contribute to generation of data with high spatial and temporal resolution. Compounds under development are of a larger molecular weight, ranging from 30–100 kDa, offer a longer blood pool residence time and permit acquisition of steady state images for more than an hour. These high molecular weight contrast agents remain intravascular in all tissues except for leaky tumor vasculature [128,129,130].

2.7.3. Kinetic Modeling of Dynamic-Contrast Enhanced MRI Data—A major difference between DCE-MRI data and data from other techniques is the fact that DCE-MRI measures the effect of the contrast agent on water relaxation and not the contrast agent itself. DCE-MR imaging enables the acquisition of a signal enhancement versus time curve, and pharmacokinetic models have been devised for quantitative evaluation of such curves to extract values for the volume transfer constant (K^{trans}) between the plasma compartment and the interstitial space and the fractional volume of the interstitial space (v_e) [131]. The rate constant, k_{ep}, is the ratio of the transfer constant to the extravascular extracellular fractional volume, v_e:

$$k_{ep}=K^{trans}/v_e. \quad \text{Equation 20}$$

This rate constant can be directly derived from the shape of the contrast agent concentration versus time curve, but access to K^{trans} and v_e require knowledge of absolute values of contrast agent concentration.

In the early part of this review, tracer uptake in the tissue was expressed as the difference between the quantity of tracer delivered to the tissue from the arterial phase (C_a) and the quantity removed by the venous phase (C_v):

$$\frac{dQ}{dt}=F(C_a-C_v). \quad \text{Equation 21}$$

If the intrinsic permeability of the capillary is high, then transport of a solute across the capillary is dependent on blood flow rather than diffusion, and as such is *flow-limited*. Tofts *et. al.* have extended this interpretation to include flow per unit mass of tissue as opposed to

total blood flow, and mass tissue concentration (C_t/ρ) instead of volume tissue concentration (C_t) [20]:

$$\frac{dC_t}{dt}=F\rho(C_a-C_v). \quad \text{Equation 22}$$

In this case, ρ (g ml^{-1}) is needed because F is now expressed in ml g^{-1} min^{-1}. The partition coefficient, λ, relates the concentration of the tracer in the tissue to the concentration of the tracer in the blood:

$$C_t=\lambda C_v. \quad \text{Equation 23}$$

It then follows that:

$$\frac{dC_t}{dt}=-\frac{F}{\lambda}(C_t-\lambda\rho C_a). \quad \text{Equation 24}$$

In a flow-limited regime, the venous plasma concentration $C_v/(1-Hct)$ can be assumed equal to the concentration in the extravascular extracellular space (C_e). λ is derived in terms of v_e, and the final model is expressed as:

$$\frac{dC_t}{dt}=F\rho(1-Hct)(C_p-C_t/v_e). \quad \text{Equation 25}$$

This model is used in situations where capillary permeability to the contrast agent is very high (i.e. when small molecular weight contrast agents are used). The rate of uptake of the contrast agent into the tissue is related to the v_e and the contrast agent concentrations in the tissue (C_t) and the arterial blood plasma (C_p). Importantly, the transfer constant, K^{trans}, is a function of the perfusion of whole blood per unit mass of tissue (F, ml g^{-1} min-^{1}), the density of tissue (ρ, g ml-^{1}) and the hematocrit (Hct) (i.e. $K^{trans}= F\rho(1- Hct)$).

In situations where capillary permeability to the contrast agent is very low (i.e. when high molecular weight contrast agents are used), K^{trans} is a function of the permeability surface area product (PS, ml min-^{1} g-^{1}) of the capillary wall and ρ, (i.e. $K^{trans}= PS\rho$), and the rate of uptake is related to the v_e, C_t and C_p:

$$\frac{dC_t}{dt}=PS\rho(C_p-C_t/v_e). \quad \text{Equation 26}$$

Finally, in situations where capillary permeability is intermediate, K^{trans} is equal to the fractional reduction in capillary blood concentration during the passage of the contrast agent through the tissue, or the extraction ratio (E) and the hematocrit (i.e. $K^{trans}= EF\rho$), and the rate of uptake is related to the v_e, C_t, and C_p:

$$\frac{dC_t}{dt} = EF\rho(1-Hct)(C_p - C_t/v_e). \quad \text{Equation 27}$$

In summary, the contrast agent concentration kinetics are a function of the plasma concentration, K^{trans} and v_e, or K^{trans} and k^{ep}. This is expressed by a generalized form for each of the three previous models:

$$\frac{dC_t}{dt} = K^{trans}(C_p - C_t/v_e) = K^{trans}C_p - k_{ep}C_t, \quad \text{Equation 28}$$

which describes the change in the concentration of the contrast agent as a function of time in terms of K^{trans} and v_e. It is important to note here that each model (high, low or intermediate capillary permeability to contrast agent) ignore the contribution of intravascular contrast agent to tissue concentration, and therefore, limit the fitted model parameters to only K^{trans} and v_e. Contrast agents of different molecular weights will require the use of different models for permeability. Of the listed parameters, C_p and C_t are actually measured and K^{trans}, k_{ep} and v_e are calculated from the fitted model equations.

3 Antiangiogenic & Antivascular Therapies

3.1 Antivascular vs. Antiangiogenic Therapies

Antivascular therapies target an established vessel network. In general, they induce collapse of a mature vasculature, reduce perfusion, blood volume and vascular tortuosity [132]. Available antivascular therapies have been tabulated:

Antivascular Agents		
Drug	**Target**	**General Mechanism of Action**
Combretastatin A4 phosphate	Tubulin	Disrupts tubulin cytoskeleton, induces rapid vascular shutdown
N-Acetylcolchinol-*O*-Phosphate (ZD6126)	Tubulin	Disrupts tubulin cytoskeleton, changes in cell morphology of proliferating endothelial cells
5,6-dimethylxanthenone-4-acetic acid (DMXAA)	Host immune system	Stimulation of host immune system, induction of vascular collapse

Antiangiogenic therapies, on the other hand, target actively proliferating and newly forming vessel networks. Most antiangiogenic therapies are small molecule inhibitors of vascular growth factors that support the neovasculature. In general, antiangiogenic therapies reduce permeability, perfusion and blood volume.

Antiangiogenic Agents		
Drug	**Target**	**General Mechanism of Action**
AEE788	VEGFR-1 & -2, EGFR	Dual inhibitor of EGFR and VEGFR

Antiangiogenic Agents		
Drug	**Target**	**General Mechanism of Action**
Vandetanib (ZD6474)	VEGFR-2, EGFR, FGFR-1, RET	Dual inhibitor of EGFR and VEGFR
Axitinib (AG-013736)	VEGFR-1, -2 & -3, PDGFR-β, c-Kit	Inhibits VEGFR autophosphorylation, inhibits endothelial cell proliferation and survival
Sunitinib (SU11248)	VEGFR-1, -2 & -3, PDGFR-β, c-Kit	Inhibits endothelial cell proliferation and survival
Recentin (AZD2171)	VEGFR-1, -2 & -3, PDGFR-β, c-Kit	Inhibits VEGF-induced angiogenesis *in vivo*
Vatalanib (PTK787/ZK222584)	VEGFR-1, -2 & -3, PDGFR-β, c-Kit	Inhibits endothelial cell proliferation and survival
Sorafenib (BAY 43-9006)	VEGFR-2 & -3, Raf kinase, PDGFR-β, c-	Inhibits tumor and endothelial cell proliferation and survival
O-(chloro-acetyl-carbamoyl) (TNP-470/AGM-1470)	Kit, RET EC growth	Relatively specifically cytostatically inhibits endothelial cell growth (UI 8297716)
PX-866	PI3-Kinase	Inhibits PI-3-kinase pathway, cellular proliferation and survival
LY294002	PI3-Kinase	Inhibits PI-3-kinase pathway, cellular proliferation and survival
Wortmannin	PI3-Kinase	Inhibits PI-3-kinase pathway, cellular proliferation and survival
Bevacizumab (rhuMAb VEGF)	VEGF	Monoclonal antibody to VEGF
Volociximab	AAB1	targets AAB1, a component protein of α5β1
HuMV833	VEGF	recombinant humanized IgG4k monoclonal antibody targeting VEGF
“VEGF-trap” (AVE 0005)	VEGF	Fusion of human IgG1 Fc to extracellular domains of VEGFR-1 and VEGFR-2; binds VEGF
IMC-1121B (anti-VEGFR-2MAb)	VEGF-R2	IgG antibody targeting VEGFR-2
Endostatin	α5β1, αvβ3 & αvβ5	Interferes with migration and proliferation of endothelial cell
Tumstatin	αvβ3	Inhibits EC protein synthesis
Angiostatin	Integrin αvβ3	Competitively binds to integrins, inhibiting interaction with matrix ligands, interfering w/cell attachment and adhesion
Neovastat	MMPs	Inhibition of MMPs

The table of antiangiogenic inhibitors above is a conglomeration of direct and indirect inhibitors. Indirect inhibitors of angiogenesis target tumor cell production of angiogenic growth factors and their receptors. This type of inhibitor is prone to development of resistance as there is a substantial opportunity for the cell to pursue alternative pathways of angiogenesis. Direct inhibitors of angiogenesis target tumor endothelial cells and inhibit endothelial cell proliferation, migration, tube formation and/or induce endothelial cell apoptosis [133].

Successful clinical trial design for conventional cytotoxic agents is based on the following concepts: 1) the agent is associated with a dose-dependent toxicity; 2) an upper limit for dose-escalation will be set by a dose-limiting toxicity (DLT) (e.g. anemia); 3) the maximum

tolerated dose (MTD) has the highest probability of producing objective remission (shrinking the tumor) and improving palliation of symptoms and; 4) the agent, alone or in combination, is capable of prolonging survival. The standard paradigm for selecting the dose of chemotherapeutic agents, the MTD, is not appropriate for antiangiogenic drugs because a) as these are targeted therapies, the optimal dose may be much less than the tolerated dose, b) they are associated with low incidence of side-effects and; c) the DLT may not be biochemically related to the agent's mechanism of action. Since antiangiogenic and antivascular therapies are cytostatic, measuring tumor volumes is impractical because tumor shrinkage or disease progression may not occur or could take weeks or months to be visible. Furthermore, heterogeneity in individual responses to cytostatic therapies would require large populations to obtain significance, leading to long and expensive clinical trials. Therefore, many potential antiangiogenic therapies have not lived up to the expectations of preclinical trials, in part because of the difficulties in designing clinical trials for antiangiogenic drugs.

Thus, there is a need to establish sensitive and reliable biomarkers of early responses to antiangiogenic or antivascular drugs, for *in vivo* pharmacodynamics (i.e. action of a drug on its target). Drug action can then be compared to subsequent clinical responses to ascertain if it is effective. Because antiangiogenic or antivascular therapies are designed to affect the abnormal blood vessels recruited by tumors, changes in blood volume, blood flow, or other hemodynamic parameters may be promising biomarkers that allow for an *in vivo* assessment of the biological activity of these angiogenic modulators.

3.2 Table: Imaging Response to Antivascular vs. Antiangiogenic Therapies

Methodological details about the imaging methods that have exploited these physiological parameters are described elsewhere in this review. However, the following table presents a list of pre-clinical studies and clinical trials that have used these modalities to evaluate the effects of several important antiangiogenic or antivascular therapies:

Drug	Imaging Study	Reference
CA4P	PET- Perfusion	[66]
Razoxane	PET - Perfusion and blood volume	[67]
SU5416	PET - Perfusion and metabolism	[68]
Bevacizumab	CT - Perfusion	[88]
MEDI-522	CT - Blood flow, blood volume, PS, MTT	[89]
AZD2171	DCE-MRI – Decreases in K^{trans}	[134,135]
SU11248	DCE-MRI – Decreases in K^{trans} & fPV 24h post-treatment	[136]
AG-013736	DCE-MRI – Decreases in K^{trans} 48h post-treatment	[137]
PTK787/ZK222584	DCE-MRI – Dose dependent reduction in K^{trans} & AUC	[138,139]
AEE788	DCE-MRI – Decrease in area under enhancement curve	[140]
ZD6474	DCE-MRI – Dose dependent reduction in K^{trans}	[141]
HuMV833	DCE-MRI – Decreases in K^{trans} 48h post-treatment	[142]
Endostatin	DCE-MRI – No consistent change in K^{trans} or v_e	[143]

4 Remaining Questions: Endothelial Transport of Contrast Agents

4.1 Mechanisms Macromolecular Transport

Thus far, we have discussed the mechanisms regulating ion and small molecule transport through passive mechanisms, though it was indicated that active transport mechanisms may be regulating transport as well. Indeed, the concept of the endothelium as a passive, simple barrier to blood constituents has long since been replaced with the idea of an endothelium that can sense, modulate and control macromolecular transport. This section will focus on the transport of macromolecules and the characteristics that determine capillary permeability to these macromolecules.

The consensus among morphologists is that large molecules require a transcytotic event or active, transcellular shuttle mechanism to get from the luminal end to the abluminal end and vice versa. The first system proposed described the shuttling of plasmalemmal vesicles or caveolae across the endothelial cells between the luminal and abluminal ends [144]. An alternative form of transport is mediated by so-called “vesicular-vacuolar organelles” (VVO), which create transendothelial channels that span the luminal to the abluminal end [145]. Independent observation of a membrane-bound tubular system evidently used for transport sparked a debate as to whether or not all three systems were describing the same phenomena [146].

The regulation of transport naturally begins at the level of the luminal plasmalemma. As the forefront of the transport process, this luminal membrane interacts with all blood constituents and functions in sorting these molecules to the designated location. The luminal plasmalemmal surface is comprised of glycoconjugates (e.g. glycoproteins, glycolipids and proteoglycans), enzymes (e.g. lipoprotein lipase and angiotensin convertin enzymes) and receptors for specific plasma molecules (e.g. vasoactive amines, hormones, procoagulants, anticoagulants, carrier proteins and lipoproteins) [147]. This expression profile differs significantly from the abluminal surface of the plasmalemma, suggesting that the cell surface protein distribution of both interfaces is important for moving blood constituents either from the luminal compartment of the capillary to the interstitial compartment in the tissue or from the interstitial compartment to the lumen of the capillary [148].

Independent transport mechanisms mediate the trafficking of materials across the plasma membrane. The functional units of these mechanisms, including interendothelial junctions (paracellular transport), caveolae (transcytosis) and their transendothelial channels, and vesiculo-vacuolar organelles (VVO), are diagrammed in Figure 2 and discussed in greater detail below.

4.1.1. Paracellular Transport—Paracellular transport can be described as transport through the interendothelial junctions between adjacent endothelial cells. This system limits transport to ions with radii less than 3 nm, such as urea, glucose and small ions. However, under certain conditions, these tightly regulated interendothelial junctions will transform to allow intercellular gaps to form, through which select macromolecules like plasma proteins can pass into the extravascular extracellular space [148,149]. This process is mediated by binding of VEGF and certain inflammatory mediators to their receptors.

4.1.2. Transcellular Transport—Transcellular transport or transcytosis describes the process whereby molecules are translocated across the cell to the interstitial fluid. Transcytosis can occur via non-specific mechanisms (fluid phase and/or adsorptive) or specific mechanisms (receptor-mediated) [148]. The process of fluid phase transcytosis is described as endocytosis of the plasma by caveolae and the subsequent relocation of the contents to the abluminal surface where the vesicle is disencumbered. Adsorptive nonspecific transcytosis involves an electrostatic interaction between the vesicle and the molecule before the translocation event can occur. Specific transcytosis is entirely receptor-mediated.

4.1.2.1. Caveolae: Caveolae are small vesicles (mean diameter ~70 nm) that are open to the endothelial cell membrane on either end—luminal or abluminal—via a thin neck of 10–40 nm in diameter, endowing them with the “flask-shape” distinction often referred to in the literature. The aperture between the endothelial cell membrane and the caveolae is sometimes enclosed by a thin diaphragm displaying a central knob and spoke-like features, which act as a size and ion filter [150,151]. These vesicles have been implicated in endocytotic and transcytotic transport mechanisms. The latter of the two will be described in more detail. A review on the endocytotic transport pathway can be found elsewhere [133].

Caveolae have a heavy lipid composition, particularly, sphingomyelin and cholesterol. The expression of caveolin-1 is also an integral part of the caveolar composition. This protein mediates protein-protein interaction with G-protein subunits, Ha-Ras, Src tyrosine kinases and eNOS [152].

4.1.2.2. Transendothelial Channels: The original postulation for transendothelial channels was not married to substantial evidence for their existence [151] until years later when it was evidenced more clearly [153]. These channels are created when a sequence of caveolae line up from one end of the plasma membrane to the other to form an open channel. It is presumed that these structures regulate function by providing a dynamic hydrophobic channel or pore.

4.1.2.3. Vacuolar Organelles: Vesiculo-vacuolar organelles are clusters of vesicles that can arrange into continuous channels that span across the endothelial cell membrane, and in some cases, have been observed spanning to the lateral endothelial cell interface. It is not entirely clear whether they are morphologically distinct from transendothelial channels (AL Baldwin, personal communication). Nevertheless, they were originally described by Dvorak’s group [145,154] and have been reported elsewhere [155,156,157]. The size of these vesicles can range from 80–140 nm in diameter. They are clusters of smaller vesicles that are 1–2 μm in the longest dimension. They are hypothesized to have some involvement in the transportation of large molecules because treatment of normal animals with a permeabilizing agent resulted in an increased extravasation of ferritin in normal venules by way of VVO structures [158]. VVO structures also contain diaphragms that separate the luminal and abluminal interfaces from the interior of the vesicle. The only aspect that seems to significantly deviate from a caveolin-like morphology is that the behavior of these vesicles is completely normal in caveolin-deficient mice, indicating that these structures do not require caveolin-1 for function [159,160].

5 Conclusions

This review has described both the physical basis of microvascular permeability as well as the mathematical methods required for a clinically practical imaging approach to estimating this parameter. It has presented methods that the imaging community has developed to deliver an estimation of microvascular permeability in the attempt to establish reliable and sensitive measures of response to therapy in human tumors. It is anticipated that microvascular permeability will evolve into a clinically useful biomarker that can 1) aid in the "Go/No Go" decision making process in drug development; 2) become a useful tool in establishing a drug's mechanism of action and; 3) ultimately transform into a surrogate endpoint for drug approval purposes. A logical initiation point for this review was to define vascular permeability and perfusion, diagram major vessel architecture and mammalian regulation of blood flow, and survey the various morphologies of capillaries and modes of transport, both passive and active. In order to associate microvascular permeability with angiogenesis, mechanisms of normal physiological and tumor angiogenesis were described canvassing the litany of *in vitro* and *in vivo* assays used to observe angiogenesis. These issues provided a reasonable segue into the current status of clinical imaging of perfusion, blood flow, permeability, distribution and vascular volumes using PET, SPECT, DCE-MRI, ultrasound and optical imaging, particularly in the context of their ability to estimate tumor response to antiangiogenic and antivascular therapies.

There is no 'silver bullet' or best method for quantifying microvascular hemodynamics. No standard protocols for measuring microvascular hemodynamics exist and reproducibility is simply not adequate across image sites and different imaging centers. Perhaps a profile of hemodynamic data obtained by an array of imaging assays would lead to more reliable and robust indicators of therapy response than any one imaging modality could alone provide. Nevertheless, the contribution of each modality as an adjuvant to traditional tumor response indices is powerful and unrefuted. At the very least, researchers interested in progressing a particular technique alone or in combination with other imaging modalities will continue to find fellowship in this large community of hypothesis-generating studies.

Abbreviations used in this paper

Ang-1 & 2	angiopoietin 1 & 2
AUC	area under the curve
bFGF	basic fibroblast growth factor
CA4P	combrestatin A4 phosphate
CAM	chick chorioallantoic membrane
CT	Computed Tomography
DCE-MRI	Dynamic-Contrast Enhanced Magnetic Resonance Imaging
ECM	extracellular matrix
EES	extracellular extravascular space

GM	Gliobastoma multiforme
MMP	matrix metalloproteinases
MTT	mean transit time
NSCLC	Non-small cell lung cancer
PET	Positron Emission Tomography
PS	permeability surface area product
RBCs	red blood cells
SCLC	Small cell lung cancer
SPECT	Single-Photon Emission Computed Tomography
tPA	tissue plasminogen activator
uPA	urokinase-type plasminogen activator
VEGF	Vascular endothelial growth factor
VEGF-R1 and -R2	VEGF-Receptor 1 and 2
CW Doppler	continuous-wave Doppler
CEUS	contrast-enhanced ultrasound
DOT	Diffuse Optical Tomography
HMWCA	high molecular weight contrast agents
SMWCA	small molecular weight contrast agents

References

1. Sherwood, L. Human Physiology. 4. Brooks/Cole Publishing; 2001.
2. Patton, HD.; Fuchs, AF.; Hille, B.; Scher, AM.; Steiner, R. Textbook of Physiology: Circulation, Respiration, Body Fluids, Metabolism and Endocrinology. 21. Philadelphia: W.B. Saunders Company, Harcourt Brace Jovanocivh, Inc; 1989.
3. Oh P, Li Y, Yu J, Durr E, Krasinska KM, Carver LA, Testa JE, Schnitzer JE. Subtractive proteomic mapping of the endothelial surface in lung and solid tumours for tissue-specific therapy. [see comment]. Nature. 2004; 429:629–635. [PubMed: 15190345]
4. Durr E, Yu J, Krasinska KM, Carver LA, Yates JR, Testa JE, Oh P, Schnitzer JE. Direct proteomic mapping of the lung microvascular endothelial cell surface in vivo and in cell culture. Nature Biotechnology. 2004; 22:985–992.
5. Kety SS. The theory and applications of the exchange of inert gas at the lungs and tissues. Pharmacological Reviews. 1951; 3:1–41. [PubMed: 14833874]
6. Murray, PDF. The development in vitro of the early chick embryo. Strangeways Research Laboratory Cambridge; 1932. p. 497-521.
7. Pardanaud L, Luton D, Prigent M, Bourcheix LM, Catala M, Dieterlen-Lievre F. Two distinct endothelial lineages in ontogeny, one of them related to hemopoiesis. Development. 1996; 122:1363–1371. [PubMed: 8625825]
8. Palis J, McGrath KE, Kingsley PD. Initiation of hematopoiesis and vasculogenesis in murine yolk sac explants. Blood. 1995; 86:156–163. [PubMed: 7795222]

9. Mills KR, Kruep D, Saha MS. Elucidating the origins of the vascular system: a fate map of the vascular endothelial and red blood cell lineages in Xenopus laevis. Developmental Biology. 1999; 209:352–368. [PubMed: 10328926]
10. Risau W, Flamme I. Vasculogenesis. [Review] [122 refs]. Annual Review of Cell & Developmental Biology. 1995; 11:73–91.
11. Ferguson JE III, Kelley RW, Patterson C. Mechanisms of endothelial differentiation in embryonic vasculogenesis. [Review] [107 refs]. Arteriosclerosis, Thrombosis and Vascular Biology. 2005; 25:2246–2254.
12. Tonnesen MG, Feng X, Clark RA. Angiogenesis in wound healing. [Review] [65 refs]. Journal of Investigative Dermatology, Symposium Proceedings. 2000; 5:40–46.
13. Reynolds LP, Killilea SD, Redmer DA. Angiogenesis in the female reproductive system. [Review] [66 refs]. FASEB Journal. 1992; 6:886–892. [PubMed: 1371260]
14. Li WW. Angiogenesis in wound healing. Contemporary Surgery, Supplement. 2003:1–36.
15. Hanahan D, Weinberg RA. The hallmarks of cancer. [Review] [94 refs]. Cell. 2000; 100:57–70. [PubMed: 10647931]
16. Schlatter P, Konig MF, Karlsson LM, Burri PH. Quantitative study of intussusceptive capillary growth in the chorioallantoic membrane (CAM) of the chicken embryo. Microvascular Research. 1997; 54:65–73. [PubMed: 9245646]
17. Risau W. Mechanisms of angiogenesis. [Review] [53 refs]. Nature. 1997; 386:671–674. [PubMed: 9109485]
18. Djonov V, Schmid M, Tschanz SA, Burri PH. Intussusceptive angiogenesis: its role in embryonic vascular network formation. Circulation Research. 2000; 86:286–292. [PubMed: 10679480]
19. Djonov V, Baum O, Burri PH. Vascular remodeling by intussusceptive angiogenesis. [Review] [59 refs]. Cell and Tissue Research. 2003; 314:107–117. [PubMed: 14574551]
20. Liekens S, De Clercq E, Neyts J. Angiogenesis: regulators and clinical applications. [Review] [225 refs]. Biochemical Pharmacology. 2001; 61:253–270. [PubMed: 11172729]
21. Kalluri R. Basement membranes: structure, assembly and role in tumour angiogenesis. Nature Reviews, Cancer. 2003; 3:422–433. [Review] [221 refs].
22. Conway EM, Collen D, Carmeliet P. Molecular mechanisms of blood vessel growth. [Review] [140 refs]. Cardiovascular Research. 2001; 49:507–521. [PubMed: 11166264]
23. Carmeliet P. Mechanisms of angiogenesis and arteriogenesis. [Review] [71 refs]. Nature Medicine. 2000; 6:389–395.
24. Thurston G, Rudge JS, Ioffe E, Zhou H, Ross L, Croll SD, Glazer N, Holash J, McDonald DM, Yancopoulos GD. Angiopoietin-1 protects the adult vasculature against plasma leakage. Natural Medicines. 2000; 6:460–463.
25. Lijnen HR. Extracellular proteolysis in the development and progression of atherosclerosis. [Review] [49 refs]. Biochemical Society Transactions. 2002; 30:163–167. [PubMed: 12023844]
26. Bischoff J. Cell adhesion and angiogenesis. [Review] [27 refs]. Journal of Clinical Investigation. 1997; 100:S37–S39. [PubMed: 9413399]
27. Papetti M, Herman IM. Mechanisms of normal and tumor-derived angiogenesis. [Review] [266 refs]. American Journal of Physiology - Cell Physiology. 2002; 282:C947–C970. [PubMed: 11940508]
28. Sandison JC. A new method for the microscopic study of living growing tissues by introduction of a transparent chamber in the rabbit's ear. Anatomical Record. 1924; 28:281–287.
29. Greenblatt M, Shubi P. Tumor angiogenesis: transfilter diffusion studies in the hamster by the transparent chamber technique. Journal of the National Cancer Institute. 1968; 41:111–124. [PubMed: 5662020]
30. Algire GH, Chalkley HW. Vascular reactions of normal and malignant tissues in vivo. Journal of the National Cancer Institute. 1945; 3:73–85.
31. Algire GH. An adaptation of the transparent chamber technique to the mouse. Journal of the National Cancer Institute. 1943; 4:1–11.

32. Yuan F, Salehi HA, Boucher Y, Vasthare US, Tuma RF, Jain RK. Vascular permeability and microcirculation of gliomas and mammary carcinomas transplanted in rat and mouse cranial windows. Cancer Research. 1994; 54:4564–4568. [PubMed: 8062241]
33. Dellian M, Witwer BP, Salehi HA, Yuan F, Jain RK. Quantitation and physiological characterization of angiogenic vessels in mice: effect of basic fibroblast growth factor, vascular endothelial growth factor/vascular permeability factor, and host microenvironment.[see comment]. American Journal of Pathology. 1996; 149:59–71. [PubMed: 8686763]
34. Auerbach R, Akhtar N, Lewis RL, Shinners BL. Angiogenesis assays: problems and pitfalls. [Review] [30 refs]. Cancer and Metastasis Reviews. 2000; 19:167–172. [PubMed: 11191056]
35. Heuser LS, Miller FN. Differential macromolecular leakage from the vasculature of tumors. Cancer. 1986; 57:461–464. [PubMed: 2417677]
36. Zeidman I. The fate of circulating tumors cells. I. Passage of cells through capillaries. Cancer Research. 1961; 21:38–39. [PubMed: 13788099]
37. Jain RK, Schlenger K, Hockel M, Yuan F. Quantitative angiogenesis assays: progress and problems. [Review] [82 refs]. Nature Medicine. 1997; 3:1203–1208.
38. Nguyen M, Shing Y, Folkman J. Quantitation of angiogenesis and antiangiogenesis in the chick embryo chorioallantoic membrane. Microvascular Research. 1994; 47:31–40. [PubMed: 7517489]
39. Auerbach R, Arensman R, Kubai L, Folkman J. Tumor-induced angiogenesis: lack of inhibition by irradiation. International Journal of Cancer. 1975; 15:241–245.
40. Gimbrone MA Jr, Leapman SB, Cotran RS, Folkman J. Tumor dormancy in vivo by prevention of neovascularization. Journal of Experimental Medicine. 1972; 136:261–276. [PubMed: 5043412]
41. Langer R, Brem H, Falterman K, Klein M, Folkman J. Isolations of a cartilage factor that inhibits tumor neovascularization. Science. 1976; 193:70–72. [PubMed: 935859]
42. Akhtar N, Dickerson EB, Auerbach R. The sponge/Matrigel angiogenesis assay. Angiogenesis. 2002; 5:75–80. [PubMed: 12549862]
43. Passaniti A, Taylor RM, Pili R, Guo Y, Long PV, Haney JA, Pauly RR, Grant DS, Martin GR. A simple, quantitative method for assessing angiogenesis and antiangiogenic agents using reconstituted basement membrane, heparin, and fibroblast growth factor. Laboratory Investigation. 1992; 67:519–528. [PubMed: 1279270]
44. Weidner N, Semple JP, Welch WR, Folkman J. Tumor angiogenesis and metastasis--correlation in invasive breast carcinoma. New England Journal of Medicine. 1991; 324:1–8. [PubMed: 1701519]
45. Srivastava A, Laidler P, Hughes LE, Woodcock J, Shedden EJ. Neovascularization in human cutaneous melanoma: a quantitative morphological and Doppler ultrasound study. European Journal of Cancer & Clinical Oncology. 1986; 22:1205–1209. [PubMed: 2434333]
46. Louvar E, Littrup PJ, Goldstein A, Yu L, Sakr W, Grignon D. Correlation of color Doppler flow in the prostate with tissue microvascularity. Cancer. 1998; 83:135–140. [PubMed: 9655303]
47. Cosgrove DO, Bamber JC, Davey JB, McKinna JA, Sinnett HD. Color Doppler signals from breast tumors. Work in progress. Radiology. 1990; 176:175–180. [PubMed: 2191364]
48. Adler DD, Carson PL, Rubin JM, Quinn-Reid D. Doppler ultrasound color flow imaging in the study of breast cancer: preliminary findings. Ultrasound in Medicine and Biology. 1990; 16:553–559. [PubMed: 2238263]
49. Koch AE. Review: angiogenesis: implications for rheumatoid arthritis. [Review] [104 refs]. Arthritis & Rheumatism. 1998; 41:951–962. [PubMed: 9627005]
50. Sebag J, McMeel JW. Diabetic retinopathy. Pathogenesis and the role of retina-derived growth factor in angiogenesis. [Review] [86 refs]. Survey of Ophthalmology. 1986; 30:377–384. [PubMed: 2425445]
51. Creamer D, Sullivan D, Bicknell R, Barker J. Angiogenesis in psoriasis. [Review] [37 refs]. Angiogenesis. 2002; 5:231–236. [PubMed: 12906316]
52. Majno G. Chronic inflammation: links with angiogenesis and wound healing. [comment] [Review] [27 refs]. American Journal of Pathology. 1998; 153:1035–1039. [PubMed: 9777935]
53. Ryschich E, Schmidt J, Hammerling GJ, Klar E, Ganss R. Transformation of the microvascular system during multistage tumorigenesis. International Journal of Cancer. 2002; 97:719–725.

54. Holash J, Wiegand SJ, Yancopoulos GD. New model of tumor angiogenesis: dynamic balance between vessel regression and growth mediated by angiopoietins and VEGF. [Review] [36 refs]. Oncogene. 1999; 18:5356–5362. [PubMed: 10498889]
55. Folkman J, Watson K, Ingber D, Hanahan D. Induction of angiogenesis during the transition from hyperplasia to neoplasia. Nature. 1989; 339:58–61. [PubMed: 2469964]
56. Carmeliet P, Jain RK. Angiogenesis in cancer and other diseases. [Review] [75 refs]. Nature. 2000; 407:249–257. [PubMed: 11001068]
57. Weidner N. Tumour vascularity and proliferation: clear evidence of a close relationship. [comment]. Journal of Pathology. 1999; 189:297–299. [PubMed: 10547589]
58. Fox SB. Tumour angiogenesis and prognosis. [see comment] [Review] [112 refs]. Histopathology. 1997; 30:294–301. [PubMed: 9088964]
59. Gatenby RA, Gillies RJ. Why do cancers have high aerobic glycolysis? [Review] [96 refs]. Nature Reviews, Cancer. 2004; 4:891–899.
60. Krogh A. The number and distribution of capillaries in muscles with calculations of the oxygen pressure head necessary for supplying the tissue. Journal of Physiology. 1919; 52:409–415. [PubMed: 16993405]
61. Cho, ZH.; Jones, JP.; Singh, M. Foundations of Medical Imaging. 1. New York: John Wiley & Sons, Inc; 1993.
62. Yamaguchi A, Taniguchi H, Kunishima S, Koh T, Yamagishi H. Correlation between angiographically assessed vascularity and blood flow in hepatic metastases in patients with colorectal carcinoma. Cancer. 2000; 89:1236–1244. [PubMed: 11002218]
63. Wilson CB, Lammertsma AA, McKenzie CG, Sikora K, Jones T. Measurements of blood flow and exchanging water space in breast tumors using positron emission tomography: a rapid and noninvasive dynamic method. Cancer Research. 1992; 52:1592–1597. [PubMed: 1540969]
64. Hoekstra CJ, Stroobants SG, Hoekstra OS, Smit EF, Vansteenkiste JF, Lammertsma AA. Measurement of perfusion in stage IIIA-N2 non-small cell lung cancer using H(2)(15)O and positron emission tomography. Clinical Cancer Research. 2002; 8:2109–2115. [PubMed: 12114410]
65. Wells P, Jones T, Price P. Assessment of inter- and intrapatient variability in C15O2 positron emission tomography measurements of blood flow in patients with intra-abdominal cancers. Clinical Cancer Research. 2003; 9:6350–6356. [PubMed: 14695134]
66. Anderson HL, Yap JT, Miller MP, Robbins A, Jones T, Price PM. Assessment of pharmacodynamic vascular response in a phase I trial of combretastatin A4 phosphate.[see comment]. Journal of Clinical Oncology. 2003; 21:2823–2830. [PubMed: 12807935]
67. Anderson H, Yap JT, Wells P, Miller MP, Propper D, Price P, Harris AL. Measurement of renal tumour and normal tissue perfusion using positron emission tomography in a phase II clinical trial of razoxane. British Journal of Cancer. 2003; 89:262–267. [PubMed: 12865914]
68. Lara PN Jr, Quinn DI, Margolin K, Meyers FJ, Longmate J, Frankel P, Mack PC, Turrell C, Valk P, Rao J, et al. SU5416 plus interferon alpha in advanced renal cell carcinoma: a phase II California Cancer Consortium Study with biological and imaging correlates of angiogenesis inhibition. Clinical Cancer Research. 2003; 9:4772–4781. [PubMed: 14581348]
69. Miller KD, Soule SE, Calley C, Emerson RE, Hutchins GD, Kopecky K, Badve S, Storniolo A, Goulet R, Sledge GW Jr. Randomized phase II trial of the anti-angiogenic potential of doxorubicin and docetaxel; primary chemotherapy as Biomarker Discovery Laboratory. Breast Cancer Research and Treatment. 2005; 89:187–197. [PubMed: 15692762]
70. Gupta N, Saleem A, Kotz B, Osman S, Aboagye EO, Phillips R, Vernon C, Wasan H, Jones T, Hoskin PJ, Price PM. Carbogen and nicotinamide increase blood flow and 5-fluorouracil delivery but not 5-fluorouracil retention in colorectal cancer metastases in patients. Clinical Cancer Research. 2006; 12:3115–3123. [PubMed: 16707610]
71. Bruehlmeier M, Roelcke U, Schubiger PA, Ametamey SM. Assessment of hypoxia and perfusion in human brain tumors using PET with 18F-fluoromisonidazole and 15O-H2O. Journal of Nuclear Medicine. 2004; 45:1851–1859. [PubMed: 15534054]

72. Stokely EM, Sveinsdottir E, Lassen NA, Rommer P. A single photon dynamic computer assisted tomograph (DCAT) for imaging brain function in multiple cross sections. Journal of Computer Assisted Tomography. 1980; 4:230–240. [PubMed: 6965949]

73. Namba H, Yanagisawa M, Yui N, Togawa T, Kinoshita F, Iwadate Y, Sueyoshi K. Quantifying brain tumor blood flow by the microsphere model with N-isopropyl-p-[123I]iodoamphetamine super-early SPECT. Annals of Nuclear Medicine. 1996; 10:161–164. [PubMed: 8814723]

74. Andrews JC, Walker-Andrews SC, Juni JE, Warber S, Ensminger WD. Modulation of liver tumor blood flow with hepatic arterial epinephrine: a SPECT study. Radiology. 1989; 173:645–647. [PubMed: 2813766]

75. Iannotti F. Functional imaging of blood brain barrier permeability by single photon emission computerised tomography and positron emission tomography. [Review] [51 refs]. Advances & Technical Standards in Neurosurgery. 1992; 19:103–119. [PubMed: 1418118]

76. Seo Y, Fukuoka S, Nakagawara J, Takanashi M, Suematsu K, Nakamura J. Early effects of gamma knife radiosurgery on brain metastases: assessment by 201TlCl SPECT and 99mTc-DTPA-human serum albumin SPECT. Neurologia Medico-Chirurgica. 1997; 37:25–30. [PubMed: 9046801]

77. Ishiyama K, Tomura N, Okada K, Nagasawa H, Sashi R, Sasaki K, Sato K, Watarai J. Evaluating benign and malignant musculoskeletal lesions with radionuclide angiography and SPECT using Tc-99m MIBI. Clinical Nuclear Medicine. 2005; 30:598–603. [PubMed: 16100476]

78. Groshar D, McEwan AJ, Parliament MB, Urtasun RC, Golberg LE, Hoskinson M, Mercer JR, Mannan RH, Wiebe LI, Chapman JD. Imaging tumor hypoxia and tumor perfusion. Journal of Nuclear Medicine. 1993; 34:885–888. [PubMed: 8389842]

79. Ohno K, Pettigrew KD, Rapoport SI. Lower limits of cerebrovascular permeability to nonelectrolytes in the conscious rat. American Journal of Physiology. 1978; 235:H299–H307. [PubMed: 696840]

80. Sahani DV, Kalva SP, Hamberg LM, Hahn PF, Willett CG, Saini S, Mueller PR, Lee TY. Assessing tumor perfusion and treatment response in rectal cancer with multisection CT: initial observations. Radiology. 2005; 234:785–792. [PubMed: 15734934]

81. Bisdas S, Baghi M, Smolarz A, Pihno NC, Lehnert T, Knecht R, Mack MG, Vogl TJ, Tuerkay S, Koh TS. Quantitative measurements of perfusion and permeability of oropharyngeal and oral cavity cancer, recurrent disease, and associated lymph nodes using first-pass contrast-enhanced computed tomography studies. Investigative Radiology. 2007; 42:172–179. [PubMed: 17287647]

82. Gandhi D, Hoeffner EG, Carlos RC, Case I, Mukherji SK. Computed tomography perfusion of squamous cell carcinoma of the upper aerodigestive tract. Initial results. Journal of Computer Assisted Tomography. 2003; 27:687–693. [PubMed: 14501359]

83. Miles KA, Leggett DA, Kelley BB, Hayball MP, Sinnatamby R, Bunce I. In vivo assessment of neovascularization of liver metastases using perfusion CT. [see comment]. British Journal of Radiology. 1998; 71:276–281. [PubMed: 9616236]

84. Dugdale PE, Miles KA, Bunce I, Kelley BB, Leggett DA. CT measurement of perfusion and permeability within lymphoma masses and its ability to assess grade, activity, and chemotherapeutic response. Journal of Computer Assisted Tomography. 1999; 23:540–547. [PubMed: 10433282]

85. Ng QS, Goh V, Fichte H, Klotz E, Fernie P, Saunders MI, Hoskin PJ, Padhani AR. Lung cancer perfusion at multi-detector row CT: reproducibility of whole tumor quantitative measurements. Radiology. 2006; 239:547–553. [PubMed: 16543594]

86. Goh V, Halligan S, Hugill JA, Bassett P, Bartram CI. Quantitative assessment of colorectal cancer perfusion using MDCT: inter- and intraobserver agreement. AJR, American Journal of Roentgenology. 2005; 185:225–231. [PubMed: 15972428]

87. Goh V, Halligan S, Hugill JA, Gartner L, Bartram CI, Goh V, Halligan S, Hugill JA, Gartner L, Bartram CI. Quantitative colorectal cancer perfusion measurement using dynamic contrast-enhanced multidetector-row computed tomography: effect of acquisition time and implications for protocols. Journal of Computer Assisted Tomography. 2005; 29:59–63. [PubMed: 15665684]

88. Koukourakis MI, Mavanis I, Kouklakis G, Pitiakoudis M, Minopoulos G, Manolas C, Simopoulos C. Early antivascular effects of bevacizumab anti-VEGF monoclonal antibody on colorectal

carcinomas assessed with functional CT imaging. American Journal of Clinical Oncology. 2007; 30:315–318. [PubMed: 17551312]

89. McNeel DG, Eickhoff J, Lee FT, King DM, Alberti D, Thomas JP, Friedl A, Kolesar J, Marnocha R, Volkman J, et al. Phase I trial of a monoclonal antibody specific for alphavbeta3 integrin (MEDI-522) in patients with advanced malignancies, including an assessment of effect on tumor perfusion. Clinical Cancer Research. 2005; 11:7851–7860. [PubMed: 16278408]
90. Johnson JA, Wilson TA. A model for capillary exchange. American Journal of Physiology. 1966; 210:1299–1303. [PubMed: 5923068]
91. St Lawrence KS, Lee TY. An adiabatic approximation to the tissue homogeneity model for water exchange in the brain: I. Theoretical derivation. Journal of Cerebral Blood Flow and Metabolism. 1998; 18:1365–1377. [PubMed: 9850149]
92. Clark, JW.; Neuman, MR.; Olson, WH.; Peura, RA.; Primiano, FP.; Siedband, MP.; Webster, JW.; Wheeler, LA.; John, GW. Medical Instrumentation. 3. John Wiley & Sons; 1998.
93. Tanaka S, Kitamura T, Fujita M, Nakanishi K, Okuda S. Color Doppler flow imaging of liver tumors. AJR, American Journal of Roentgenology. 1990; 154:509–514. [PubMed: 2154912]
94. Bourne T, Campbell S, Steer C, Whitehead MI, Collins WP. Transvaginal colour flow imaging: a possible new screening technique for ovarian cancer.[see comment]. BMJ. 1989; 299:1367–1370. [PubMed: 2513965]
95. Rubin JM, Bude RO, Carson PL, Bree RL, Adler RS. Power Doppler US: a potentially useful alternative to mean frequency-based color Doppler US. Radiology. 1994; 190:853–856. [PubMed: 8115639]
96. Gramiak R, Shah PM. Echocardiography of the aortic root. Investigative Radiology. 1968; 3:356–366. [PubMed: 5688346]
97. Blomley MJ, Cooke JC, Unger EC, Monaghan MJ, Cosgrove DO. Microbubble contrast agents: a new era in ultrasound. [Review] [30 refs]. BMJ. 2001; 322:1222–1225. [PubMed: 11358777]
98. Lamuraglia M, Lassau N, Garbay JR, Mathieu MC, Rouzier R, Jaziri S, Roche A, Leclere J. Doppler US with perfusion software and contrast medium injection in the early evaluation of radiofrequency in breast cancer recurrences: a prospective phase II study. European Journal of Radiology. 2005; 56:376–381. [PubMed: 16005593]
99. Chaudhari MH, Forsberg F, Voodarla A, Saikali FN, Goonewardene S, Needleman L, Finkel GC, Goldberg BB. Breast tumor vascularity identified by contrast enhanced ultrasound and pathology: initial results. Ultrasonics. 2000; 38:105–109. [PubMed: 10829638]
100. Piscaglia F, Corradi F, Mancini M, Giangregorio F, Tamberi S, Ugolini G, Cola B, Bazzocchi A, Righini R, Pini P, et al. Real time contrast enhanced ultrasonography in detection of liver metastases from gastrointestinal cancer. BMC Cancer. 2007; 7:171. [PubMed: 17767722]
101. Yang W, Chen MH, Yan K, Wu W, Dai Y, Zhang H. Differential diagnosis of non-functional islet cell tumor and pancreatic carcinoma with sonography. European Journal of Radiology. 2007; 62:342–351. [PubMed: 17412543]
102. Bertolotto M, Pozzato G, Croce LS, Nascimben F, Gasparini C, Cova MA, Tiribelli C. Blood flow changes in hepatocellular carcinoma after the administration of thalidomide assessed by reperfusion kinetics during microbubble infusion: preliminary results. Investigative Radiology. 2006; 41:15–21. [PubMed: 16355035]
103. Hertz, CH. Fourth European Congress on Ultrasound in Medicine; Dubrovnik. 1981.
104. Dymling, S.; Persson, HW.; Hertz, CH. The measurement of blood perfusion in tissue. Fifth World Congress of Ultrasound in Medicine and Biology; Brighton, UK. 1982.
105. Wei K, Jayaweera AR, Firoozan S, Linka A, Skyba DM, Kaul S. Quantification of myocardial blood flow with ultrasound-induced destruction of microbubbles administered as a constant venous infusion. Circulation. 1998; 97:473–483. [PubMed: 9490243]
106. Unger EC, Matsunaga TO, McCreery T, Schumann P, Sweitzer R, Quigley R. Therapeutic applications of microbubbles. [Review] [17 refs]. European Journal of Radiology. 2002; 42:160–168. [PubMed: 11976013]
107. Unger EC, Hersh E, Vannan M, Matsunaga TO, McCreery T. Local drug and gene delivery through microbubbles. [Review] [50 refs]. Progress in Cardiovascular Diseases. 2001; 44:45–54. [PubMed: 11533926]

108. Borden MA, Martinez GV, Ricker J, Tsvetkova N, Longo M, Gillies RJ, Dayton PA, Ferrara KW. Lateral phase separation in lipid-coated microbubbles. Langmuir. 2006; 22:4291–4297. [PubMed: 16618177]

109. Borden MA, Caskey CF, Little E, Gillies RJ, Ferrara KW. DNA and polylysine adsorption and multilayer construction onto cationic lipid-coated microbubbles. Langmuir. 2007; 23:9401–9408. [PubMed: 17665937]

110. Sokolov K, Aaron J, Hsu B, Nida D, Gillenwater A, Follen M, MacAulay C, Adler-Storthz K, Korgel B, Descour M, et al. Optical systems for in vivo molecular imaging of cancer. [Review] [112 refs]. Technology in Cancer Research & Treatment. 2003; 2:491–504. [PubMed: 14640761]

111. McDevitt HO, Coons AH. Methods for preparation of fluorescent proteins. Methods in Medical Research. 1964; 10:142–148. [PubMed: 14284907]

112. Coons AH, Creech HJ, Jones RN. Immunological properties of an antibody containing a fluorescent group. Proceedings of The Society for Experimental Biology and Medicine. 1941; 42:200–202.

113. Murphy, DB. Fundamentals of Light Microscopy and Electronic Imaging. 1. New York, NY: John Wiley & Sons, Inc; 2001.

114. Weissleder R, Mahmood U. Molecular imaging. [Review] [141 refs]. Radiology. 2001; 219:316–333. [PubMed: 11323453]

115. Sadikot RT, Blackwell TS. Bioluminescence imaging. [Review] [43 refs]. Proceedings of the American Thoracic Society. 2005; 2:537–540. [PubMed: 16352761]

116. http://clinicaltrials.gov/.

117. Ntziachristos V, Chance B. Probing physiology and molecular function using optical imaging: applications to breast cancer. [Review] [29 refs]. Breast Cancer Research. 2001; 3:41–46. [PubMed: 11250744]

118. Ntziachristos V, Yodh AG, Schnall M, Chance B. Concurrent MRI and diffuse optical tomography of breast after indocyanine green enhancement. Proceedings of the National Academy of Sciences of the United States of America. 2000; 97:2767–2772. [PubMed: 10706610]

119. Brown EB, Campbell RB, Tsuzuki Y, Xu L, Carmeliet P, Fukumura D, Jain RK. In vivo measurement of gene expression, angiogenesis and physiological function in tumors using multiphoton laser scanning microscopy.[erratum appears in Nat Med 2001 Sep;7(9):1069]. Nature Medicine. 2001; 7:864–868.

120. Tozer GM, Prise VE, Wilson J, Cemazar M, Shan S, Dewhirst MW, Barber PR, Vojnovic B, Chaplin DJ. Mechanisms associated with tumor vascular shutdown induced by combretastatin A-4 phosphate: intravital microscopy and measurement of vascular permeability. Cancer Research. 2001; 61:6413–6422. [PubMed: 11522635]

121. Wu NZ, Klitzman B, Rosner G, Needham D, Dewhirst MW. Measurement of material extravasation in microvascular networks using fluorescence video-microscopy. Microvascular Research. 1993; 46:231–253. [PubMed: 8246821]

122. Hoang BH, Dyke JP, Koutcher JA, Huvos AG, Mizobuchi H, Mazza BA, Gorlick R, Healey JH. VEGF expression in osteosarcoma correlates with vascular permeability by dynamic MRI. Clinical Orthopaedics and Related Research. 2004:32–38. [PubMed: 15346048]

123. Rijpkema M, Kaanders JH, Joosten FB, van der Kogel AJ, Heerschap A. Method for quantitative mapping of dynamic MRI contrast agent uptake in human tumors. Journal of Magnetic Resonance Imaging. 2001; 14:457–463. [PubMed: 11599071]

124. Hayes C, Padhani AR, Leach MO. Assessing changes in tumour vascular function using dynamic contrast-enhanced magnetic resonance imaging. NMR in Biomedicine. 2002; 15:154–163. [PubMed: 11870911]

125. Li KL, Zhu XP, Checkley DR, Tessier JJ, Hillier VF, Waterton JC, Jackson A. Simultaneous mapping of blood volume and endothelial permeability surface area product in gliomas using iterative analysis of first-pass dynamic contrast enhanced MRI data. British Journal of Radiology. 2003; 76:39–50. [PubMed: 12595324]

126. Knopp MV, Weiss E, Sinn HP, Mattern J, Junkermann H, Radeleff J, Magener A, Brix G, Delorme S, Zuna I, van Kaick G. Pathophysiologic basis of contrast enhancement in breast tumors. Journal of Magnetic Resonance Imaging. 1999; 10:260–266. [PubMed: 10508285]

127. Turetschek K, Preda A, Novikov V, Brasch RC, Weinmann HJ, Wunderbaldinger P, Roberts TP. Tumor microvascular changes in antiangiogenic treatment: assessment by magnetic resonance contrast media of different molecular weights. Journal of Magnetic Resonance Imaging. 2004; 20:138–144. [PubMed: 15221819]

128. Raatschen HJ, Fu Y, Shames DM, Wendland MF, Brasch RC. Magnetic resonance imaging enhancement of normal tissues and tumors using macromolecular Gd-based cascade polymer contrast agents: preclinical evaluations. Investigative Radiology. 2006; 41:860–867. [PubMed: 17099424]

129. Jordan BF, Runquist M, Raghunand N, Gillies RJ, Tate WR, Powis G, Baker AF. The thioredoxin-1 inhibitor 1-methylpropyl 2-imidazolyl disulfide (PX-12) decreases vascular permeability in tumor xenografts monitored by dynamic contrast enhanced magnetic resonance imaging. Clinical Cancer Research. 2005; 11:529–536. [PubMed: 15701837]

130. Gillies RJ, Raghunand N, Karczmar GS, Bhujwalla ZM. MRI of the tumor microenvironment. [erratum appears in J Magn Reson Imaging 2002 Dec;16(6):751] [Review] [225 refs]. Journal of Magnetic Resonance Imaging. 2002; 16:430–450. [PubMed: 12353258]

131. Tofts PS, Brix G, Buckley DL, Evelhoch JL, Henderson E, Knopp MV, Larsson HB, Lee TY, Mayr NA, Parker GJ, et al. Estimating kinetic parameters from dynamic contrast-enhanced T(1)-weighted MRI of a diffusable tracer: standardized quantities and symbols. [Review] [50 refs]. Journal of Magnetic Resonance Imaging. 1999; 10:223–232. [PubMed: 10508281]

132. Leach MO, Brindle KM, Evelhoch JL, Griffiths JR, Horsman MR, Jackson A, Jayson G, Judson IR, Knopp MV, Maxwell RJ, et al. Assessment of antiangiogenic and antivascular therapeutics using MRI: recommendations for appropriate methodology for clinical trials. [Review] [10 refs]. British Journal of Radiology. 2003; 76(Spec No 1):S87–S91. [PubMed: 15456718]

133. Tandle A, Blazer DG III, Libutti SK. Antiangiogenic gene therapy of cancer: recent developments. Journal of Translational Medicine. 2006

134. Hormigo A, Gutin PH, Rafii S. Tracking normalization of brain tumor vasculature by magnetic imaging and proangiogenic biomarkers. [comment] [Review] [13 refs]. Cancer Cell. 2007; 11:6–8. [PubMed: 17222788]

135. Batchelor TT, Sorensen AG, di Tomaso E, Zhang WT, Duda DG, Cohen KS, Kozak KR, Cahill DP, Chen PJ, Zhu M, et al. AZD2171, a pan-VEGF receptor tyrosine kinase inhibitor, normalizes tumor vasculature and alleviates edema in glioblastoma patients.[see comment]. Cancer Cell. 2007; 11:83–95. [PubMed: 17222792]

136. Marzola P, Degrassi A, Calderan L, Farace P, Nicolato E, Crescimanno C, Sandri M, Giusti A, Pesenti E, Terron A, et al. Early antiangiogenic activity of SU11248 evaluated in vivo by dynamic contrast-enhanced magnetic resonance imaging in an experimental model of colon carcinoma. Clinical Cancer Research. 2005; 11:5827–5832. [PubMed: 16115922]

137. Liu G, Rugo HS, Wilding G, McShane TM, Evelhoch JL, Ng C, Jackson E, Kelcz F, Yeh BM, Lee FT Jr, et al. Dynamic contrast-enhanced magnetic resonance imaging as a pharmacodynamic measure of response after acute dosing of AG-013736, an oral angiogenesis inhibitor, in patients with advanced solid tumors: results from a phase I study. [see comment]. Journal of Clinical Oncology. 2005; 23:5464–5473. [PubMed: 16027440]

138. Thomas AL, Morgan B, Horsfield MA, Higginson A, Kay A, Lee L, Masson E, Puccio-Pick M, Laurent D, Steward WP. Phase I study of the safety, tolerability, pharmacokinetics, and pharmacodynamics of PTK787/ZK 222584 administered twice daily in patients with advanced cancer. Journal of Clinical Oncology. 2005; 23:4162–4171. [PubMed: 15867205]

139. Morgan B, Thomas AL, Drevs J, Hennig J, Buchert M, Jivan A, Horsfield MA, Mross K, Ball HA, Lee L, et al. Dynamic contrast-enhanced magnetic resonance imaging as a biomarker for the pharmacological response of PTK787/ZK 222584, an inhibitor of the vascular endothelial growth factor receptor tyrosine kinases, in patients with advanced colorectal cancer and liver metastases: results from two phase I studies. [see comment]. Journal of Clinical Oncology. 2003; 21:3955–3964. [PubMed: 14517187]

140. Traxler P, Allegrini PR, Brandt R, Brueggen J, Cozens R, Fabbro D, Grosios K, Lane HA, McSheehy P, Mestan J, et al. AEE788: a dual family epidermal growth factor receptor/ErbB2 and vascular endothelial growth factor receptor tyrosine kinase inhibitor with antitumor and antiangiogenic activity. Cancer Research. 2004; 64:4931–4941. [PubMed: 15256466]

141. Checkley D, Tessier JJ, Kendrew J, Waterton JC, Wedge SR. Use of dynamic contrast-enhanced MRI to evaluate acute treatment with ZD6474, a VEGF signalling inhibitor, in PC-3 prostate tumours. British Journal of Cancer. 2003; 89:1889–1895. [PubMed: 14612898]

142. Jayson GC, Zweit J, Jackson A, Mulatero C, Julyan P, Ranson M, Broughton L, Wagstaff J, Hakannson L, Groenewegen G, et al. Molecular imaging and biological evaluation of HuMV833 anti-VEGF antibody: implications for trial design of antiangiogenic antibodies. Journal of the National Cancer Institute. 2002; 94:1484–1493. [PubMed: 12359857]

143. Eder JP Jr, Supko JG, Clark JW, Puchalski TA, Garcia-Carbonero R, Ryan DP, Shulman LN, Proper J, Kirvan M, Rattner B, et al. Phase I clinical trial of recombinant human endostatin administered as a short intravenous infusion repeated daily.[see comment]. Journal of Clinical Oncology. 2002; 20:3772–3784. [PubMed: 12228197]

144. Palade GE. Transport in quanta across the endothelium of blood capillaries. Anatomical Record. 1960; 136:254.

145. Kohn S, Nagy JA, Dvorak HF, Dvorak AM. Pathways of macromolecular tracer transport across venules and small veins. Structural basis for the hyperpermeability of tumor blood vessels. Laboratory Investigation. 1992; 67:596–607. [PubMed: 1279271]

146. Bendayan M, Rasio EA. Evidence of a tubular system for transendothelial transport in arterial capillaries of the rete mirabile. Journal of Histochemistry and Cytochemistry. 1997; 45:1365–1378. [PubMed: 9313798]

147. Simionescu M, Simionescu N. Endothelial transport of macromolecules: transcytosis and endocytosis. A look from cell biology. [Review] [407 refs]. Cell Biology Reviews. 1991; 25:5–78. [PubMed: 1364324]

148. Simionescu M, Gafencu A, Antohe F. Transcytosis of plasma macromolecules in endothelial cells: a cell biological survey. [Review] [60 refs]. Microscopy Research and Technique. 2002; 57:269–288. [PubMed: 12112439]

149. Mehta D, Malik AB. Signaling mechanisms regulating endothelial permeability. [Review] [1112 refs]. Physiological Reviews. 2006; 86:279–367. [PubMed: 16371600]

150. Bruns RR, Palade GE. Studies on blood capillaries. II. Transport of ferritin molecules across the wall of muscle capillaries. Journal of Cell Biology. 1968; 37:277–299. [PubMed: 5656395]

151. Bruns RR, Palade GE. Studies on blood capillaries. I. General organization of blood capillaries in muscle. Journal of Cell Biology. 1968; 37:244–276. [PubMed: 5656394]

152. Okamoto T, Schlegel A, Scherer PE, Lisanti MP. Caveolins, a family of scaffolding proteins for organizing “preassembled signaling complexes” at the plasma membrane. [Review] [72 refs]. Journal of Biological Chemistry. 1998; 273:5419–5422. [PubMed: 9488658]

153. Simionescu M, Simionescu N, Palade GE. Segmental differentiations of cell junctions in the vascular endothelium. The microvasculature. Journal of Cell Biology. 1975; 67:863–885. [PubMed: 1202025]

154. Dvorak AM, Kohn S, Morgan ES, Fox P, Nagy JA, Dvorak HF. The vesiculo-vacuolar organelle (VVO): a distinct endothelial cell structure that provides a transcellular pathway for macromolecular extravasation. Journal of Leukocyte Biology. 1996; 59:100–115. [PubMed: 8558058]

155. Kumar P, Timoney JF. Histology, immunohistochemistry and ultrastructure of the equine palatine tonsil. Anatomia, Histologia, Embryologia: Veterinary Medicine Series C. 2005; 34:192–198.

156. Kumar P, Timoney JF. Histology and ultrastructure of the equine lingual tonsil. II. Lymphoid tissue and associated high endothelial venules. Anatomia, Histologia, Embryologia: Veterinary Medicine Series C. 2005; 34:98–104.

157. Caruso RA, Speciale G, Inferrera A, Rigoli L, Inferrera C. Ultrastructural observations on the microvasculature in advanced gastric carcinomas. Histology and Histopathology. 2001; 16:785–792. [PubMed: 11510968]

158. Feng D, Nagy JA, Hipp J, Dvorak HF, Dvorak AM. Vesiculo-vacuolar organelles and the regulation of venule permeability to macromolecules by vascular permeability factor, histamine, and serotonin. Journal of Experimental Medicine. 1996; 183:1981–1986. [PubMed: 8642308]

159. Minshall RD, Sessa WC, Stan RV, Anderson RG, Malik AB. Caveolin regulation of endothelial function. [Review] [57 refs]. American Journal of Physiology - Lung Cellular and Molecular Physiology. 2003; 285:L1179–L1183. [PubMed: 14604847]

160. Feng D, Nagy JA, Dvorak HF, Dvorak AM. Ultrastructural studies define soluble macromolecular, particulate, and cellular transendothelial cell pathways in venules, lymphatic vessels, and tumor-associated microvessels in man and animals. [Review] [150 refs]. Microscopy Research and Technique. 2002; 57:289–326. [PubMed: 12112440]

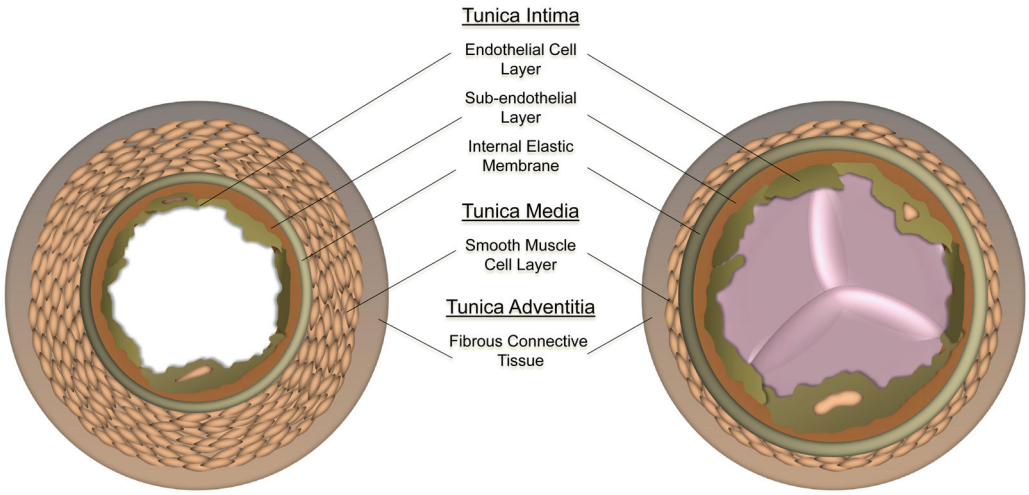

Figure 1.

Cross-sectional diagram of the distinct layers of a general artery and vein: tunica intima, media and adventitia.

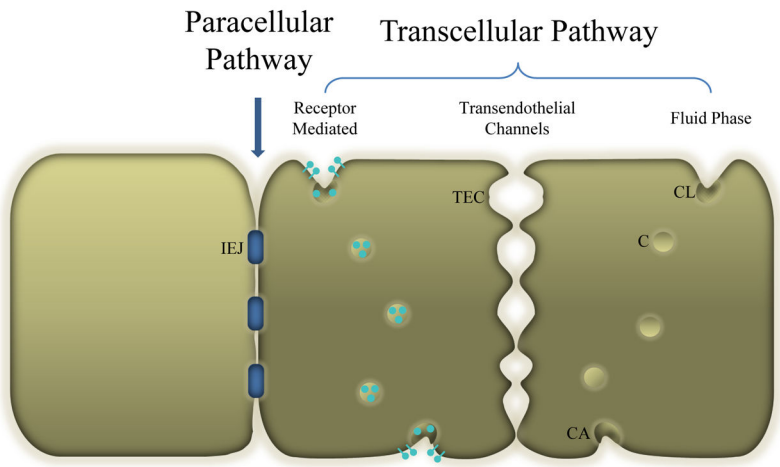

Figure 2.

Two adjacent endothelial cells separated by interendothelial cell junctions (IEJ). Endothelial cells are characterized by extensive plasmalemmal vesicles or caveolae (C). Individual caveolae can be open to the luminal front (CL) or abluminal front (CA) or free in the cytoplasm. Caveolae can aggregate end-to-end to create a transendothelial channel (TEC). The transcellular pathway mediates the transport of plasma proteins such as albumin via fluid phase or receptor mediated mechanisms, while small molecules such as glucose and urea are transported via the paracellular pathway.